

Bias in Estimators of Archaic Admixture

Alan R. Rogers^{1,*}, Ryan J. Bohlender¹

^a*Dept. of Anthropology, 270 S 1400 E, University of Utah, Salt Lake City, Utah 84112*

Abstract

This article evaluates bias in one class of methods used to estimate archaic admixture in modern humans. These methods study the pattern of allele sharing among modern and archaic genomes. They are sensitive to “ghost” admixture, which occurs when a population receives archaic DNA from sources not acknowledged by the statistical model. The effect of ghost admixture depends on two factors: branch-length bias and population-size bias. Branch-length bias occurs because a given amount of admixture has a larger effect if the two populations have been separated for a long time. Population-size bias occurs because differences in population size distort branch lengths in the gene genealogy. In the absence of ghost admixture, these effects are small. They become important, however, in the presence of ghost admixture. Estimators differ in the pattern of response. Increasing a given parameter may inflate one estimator but deflate another. For this reason, comparisons among estimators are informative. Using such comparisons, this article supports previous findings that the archaic population was small and that Europeans received little gene flow from archaic populations other than Neanderthals. It also identifies an inconsistency in estimates of archaic admixture into Melanesia.

Keywords: archaic admixture, population genetics, gene genealogy, human evolution, Neanderthal, Denisovan

1. Introduction

Forty years ago, William Howells (1976) discussed the origin of modern humans, emphasizing two extreme views. One of these, which would now be called the multiregional hypothesis (Wolpoff, 1989), held that modern humans evolved across a broad front within a worldwide population held together by gene flow. The other, which would now be called the replacement hypothesis (Stringer and Andrews, 1988), involved “a single origin, outward migration of separate stirps, like the sons of Noah, and an empty world to occupy, with no significant threat of adulteration by other gene pools or even evaporating gene puddles” (Howells, 1976, p. 480). But Howells also considered a third hypothesis, which also proposed expansion from a single point of origin. This expansion, however, involved “encounters between populations of modern man and of other forms, with consequent gene flow” (Howells, 1976, p. 492). This hypothesis has been endorsed by various paleoanthropologists (Bräuer, 1984, 1989; Smith et al., 1989; Trinkaus, 2005). During the past decade, it has also received support from genetics.

In the preceding decade, geneticists were less supportive. At that time, human evolutionary genetics dealt mainly with mitochondrial DNA (mtDNA), which is remarkably homogeneous in modern human samples. Stoneking (1993) argued that the mtDNA of Neanderthals

ought to lie well outside the narrow range of variation seen in modern human samples. The absence of such divergent mtDNAs argued that their frequency within the human species must be low. Yet as Stoneking observed, this did not refute the hypothesis of archaic admixture. Introgressed archaic mtDNAs might simply have been lost by genetic drift. Nordborg (1998) developed a model of this process, which showed that mitochondrial data have low power to detect archaic admixture.

Since the late 1990s, the field has relied increasingly on nuclear DNA. Because unlinked loci provide essentially independent replicates of the evolutionary process, the nuclear genome provides far greater power to detect admixture. A variety of statistical methods has been developed. Some rely on information in the site frequency spectrum (Eswaran et al., 2005; Yang et al., 2012). Others are based on linkage disequilibrium (Abi-Rached et al., 2011; Cox et al., 2008; Evans et al., 2005; Hammer et al., 2011; Mendez et al., 2012; Moorjani et al., 2011; Plagnol and Wall, 2006; Wall and Hammer, 2006; Wall, 2000; Wall et al., 2009).

Our focus here is on a different class of methods, which capitalizes on the availability of archaic DNA sequences. These methods infer admixture from the frequency with which derived alleles are shared by pairs of samples. In the most common pattern, the derived allele is shared by genes drawn from closely related populations. Two samples uniquely share a derived allele only if a mutation occurs in a uniquely shared ancestor. For example, at many of the loci in table 1, the derived allele is present only in the French and African samples. These derived

*Corresponding author

Email addresses: rogers@anthro.utah.edu (Alan R. Rogers), ryan.bohlender@gmail.com (Ryan J. Bohlender)

Table 1: The site patterns studied in this analysis (with 0 and 1 representing the ancestral and derived alleles); the gene tree implied by each pattern; and the counts (I_{uv}) of such sites for a San sample, x , a French sample, y , a Neanderthal sample, n , and a chimpanzee sample, o (Patterson et al., 2010a, p. S138).

Site		Gene tree	count
Pattern			
	<i>xyno</i>		
<i>ny</i>	0110	$((x, (y, n)), o)$	$I_{ny} = 103,612$
<i>nx</i>	1010	$((x, n), y), o)$	$I_{nx} = 95,347$
<i>xy</i>	1100	$((x, y), n), o)$	$I_{xy} = 303,340$

alleles arose in genes that were ancestral to the French and African samples but not to the Neanderthal or the Chimpanzee. Such sites are common in the data, because the French and African populations are conspecific and thus share a portion of their evolutionary history.

What then of the other two patterns, in which the derived allele is shared by a Neanderthal and one of the two modern human samples? In the absence of admixture, these site patterns can arise only through incomplete lineage sorting. If random mating prevailed within the population ancestral to humans and Neanderthals, these two patterns ought to occur in equal frequencies (Pamilo and Nei, 1988). Yet in table 1 the ny pattern occurs more often than the nx pattern. This excess supports the hypothesis of admixture between Neanderthals and the ancestors of Europeans. Several published methods use this principle to estimate the fraction of archaic genes in modern populations (Durand et al., 2011; Green et al., 2010; Meyer et al., 2012; Patterson et al., 2012b; Reich et al., 2010, 2011).

These methods rely on the assumption of random mating in the ancestral population. If instead that population were geographically structured, with limited gene flow between geographic subdivisions, this could result in biased frequencies such as those seen in table 1 (Slatkin and Pollack, 2008). This hypothesis of “ancestral subdivision” has been seen as an alternative to that of archaic admixture (Blum and Jakobsson, 2011; Durand et al., 2011; Eriksson and Manica, 2012). This issue is still contentious, with some authors arguing that it has been refuted (Sankararaman et al., 2012; Wall et al., 2013; Yang et al., 2012) and others that it has not been properly tested (Eriksson and Manica, 2014).

Whatever the outcome of this dispute, there are also other potential biases. Several published estimators allow for gene flow from only one archaic population. Estimates may be biased if the modern population also received genes from other archaic populations, a phenomenon known as “ghost admixture” (Beerli, 2004; Slatkin, 2005; Durand et al., 2011, p. 2240; Harris and Nielsen, 2013). Some estimators also assume that population size has been constant throughout the human gene tree. These estimators may be biased if populations have varied in size. In what follows, we explore the magnitudes of these biases.

2. Methods

Because this article is about bias, we focus on expected values and ignore statistical uncertainties. Following Durand et al. (2011, p. 2241), we assume that admixture occurs at discrete points in time. Between these events, the isolation of populations is complete. Within populations, we assume mating is at random.

2.1. Population sizes and coalescent time scale

We use single upper-case letters, such as X and Y , to label individual populations. The notation XY refers to the population ancestral to X and Y but not ancestral to other sampled populations. The diploid sizes of X , Y , and XY are written as N_X , N_Y , and N_{XY} . The symbol N_0 represents the diploid size of the the ancestral human population—the ancestors of modern humans, Neanderthals, and Denisovans, but not of chimpanzees.

In this population, the hazard of a coalescent event between a single pair of lineages is $1/2N_0$ per generation, and their mean coalescence time is $2N_0$ generations (Hudson, 1990). However, let us adopt a coalescent time scale, with time units of $2N_0$ generations. On this scale, the mean and hazard are both unity, and the mutation rate is $U \equiv 2N_0u$, where u is the mutation rate per generation.

We allow for changes in population size at branch points in the population tree. Between branching points, we assume the population is constant. For example, Fig. 1 implies that population XY existed within the time interval (ζ, λ) . Within this interval, we assume that it had constant size N_{XY} . Let $K_{XY} = N_{XY}/N_0$. In words, K_{XY} is the size of population XY relative to that of the ancestral human population. For the duration of population XY , the coalescent hazard for a single pair of lineages is $1/K_{XY}$ per unit of coalescent time. Other ratios, such as K_X and K_Y , are defined similarly.

The “survival function”, $S_{XY}^{(\zeta, \lambda)} \equiv e^{-(\lambda - \zeta)/K_{XY}}$, is the probability that a pair of lineages within XY remain distinct throughout interval (ζ, λ) . The “cumulative distribution function,” $F_{XY}^{(\zeta, \lambda)} = 1 - S_{XY}^{(\zeta, \lambda)}$, is the probability that the pair coalesces within this interval.

For a pair of lineages within population X at time t , $T_X^{(t)}$ is the expected coalescence time in units of $2N_0$ generations. It depends not only on the size of population X , but also on the sizes of populations ancestral to X . Appendix A.2 explains how $T_X^{(t)}$ is calculated. If population size is constant throughout the population tree, $K_X = T_X^{(t)} = 1$.

For numerical results, we assume the population sizes shown in table 2. The last line there is based on Gravel et al. (2011, table 2), who estimate that 932 generations ago, the European was of diploid size 1032. It then expanded exponentially at a rate of 0.0038 per generation. Over this interval, the harmonic mean population size would have been 3608. A similar calculation, based

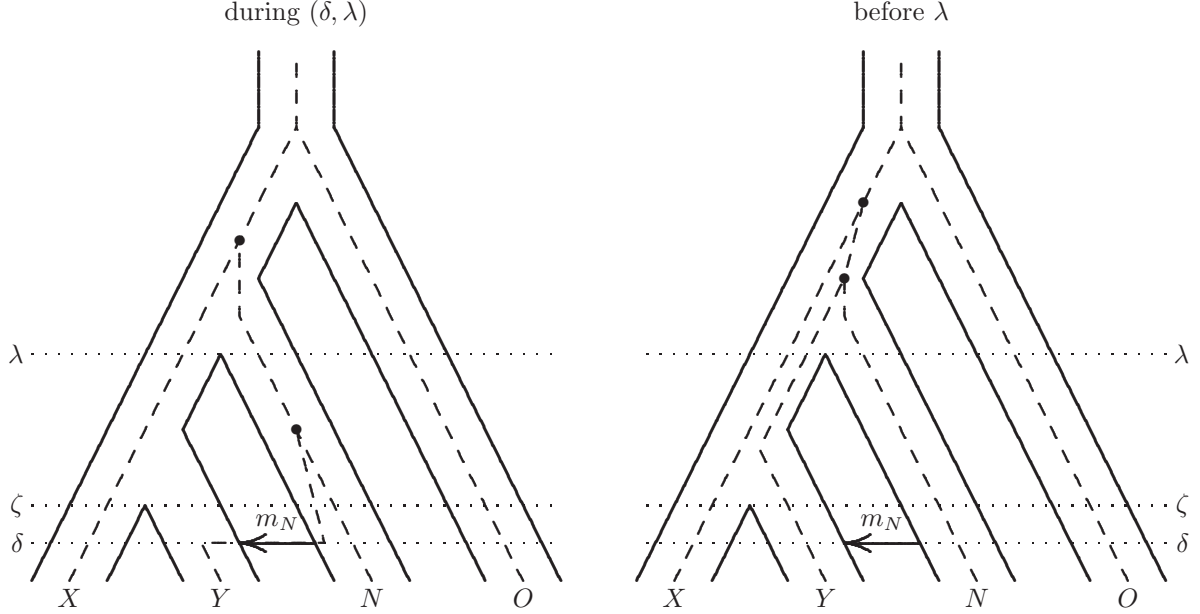


Figure 1: A population tree (solid lines) with two embedded gene trees (dashed lines). A fraction m_N of the sites in population Y descend via gene flow from population N . Greek letters δ , ζ , and λ refer to the time of the episode of gene flow, the separation of populations X and Y , and the separation of A from the two modern populations. Left panel: nucleotide carried by y is derived by gene flow from N and coalesces during (δ, λ) within population N . Right panel: nucleotide in y is native and coalesces prior to λ within ancestral human population, XYN . Bullets delineate the branches along which mutation would generate site pattern ny .

Table 2: Assumptions about population sizes

Population	Diploid size	K
Chimpanzee-human ancestor ^a	15,000	6.50
Ancestor of moderns and archaics ^b	2,308	1.00
Archaics ^b	577	0.25
Early modern humans ^b	4,615	2.00
Europe or Asia ^c	3,000	1.30

^aWall (2003); ^bPrüfer et al. (2014, Fig. 4); ^cGravel et al. (2011, table 2).

on the estimates of Gravel et al. for East Asia, gives a harmonic mean of 2446. Our own value of 3000 is a round number midway between these results. This value of 3000 was then scaled up or down to obtain lines 1–4 of table 2, the scaling ratios for lines 2–4 being chosen for consistency with Prüfer et al. (2014, Fig. 4), and that for line 1 for consistency with Wall (2003).

2.2. Site patterns and their expected frequencies

This section outlines the logic underlying the estimators that we consider below. It was introduced by Green et al. (2010) and has been used in many subsequent publications.

Consider a sample consisting of one haploid genome from each of four populations: two modern human populations, X and Y , one archaic population, N , and an outgroup, O . For example, X and Y might refer to the Yoruban and French populations, N to ancient Neanderthals, and O to chimpanzee. We use lower case

(x, y, a, o) to refer to the genomes sampled from these populations. We restrict attention to loci (nucleotide sites) at which two of the three human samples carry the derived allele, 1, and the other sample carries the ancestral allele, 0. By assumption, chimpanzee carries the ancestral allele.

Suppose that we sample one haploid genome from each population. The gene genealogy of this sample will vary from locus to locus, but many of these genealogies will have a topology similar to that of the population. We assume this topology is $((X, Y), N), O$. Many gene genealogies will however have different topologies, which may arise through incomplete lineage sorting. If the most recent coalescent event precedes the separation time, λ , of the archaic and modern populations, then there are three possible genealogies: $((x, y), n), o$, $((x, n), y), o$, and $((x, (y, n)), o)$. The right panel of Fig. 1 illustrates the last of these alternatives. If the ancestral population mated at random, the three genealogies are equally probable. In the absence of archaic admixture, two of these genealogies—the ones inconsistent with the population tree—can arise only by incomplete lineage sorting and should therefore be equally frequent. But if there were gene flow from N to Y , as seen in the left panel of Fig. 1, we’d have an excess of sites exhibiting genealogy $((x, (y, n)), o)$.

We can detect these gene genealogies only when a mutation occurs in the common ancestor either of (y, n) , of (x, n) , or of (x, y) . For example, the left panel of Fig. 2 shows the case of a site at which the nucleotide carried by y arrived via gene flow from population N . Tracing this lineage backward in time, it coalesces with n and then with x at the points marked in the figure by bullets. If

a mutation occurred between these two coalescent events, it would be shared by y and n , but not by x or o . Thus, admixture from archaic population N inflates the count of sites that exhibit pattern ny . Our goal is to use this excess to estimate the rate, m_N , of gene flow from N into Y .

Such estimates may be biased for several reasons, one of which—ghost admixture—is illustrated in Fig. 2. There, population Y receives gene flow not only from N , but also from a second archaic population, D . (The outgroup is omitted from this figure for simplicity.) As the figure illustrates, *both* forms of archaic admixture can inflate the count of site pattern ny . For this reason, ghost admixture may bias our estimate of m_N .

To describe these effects, we introduce a new notation. Let I_{ny} represent the number of sites exhibiting pattern ny , i.e. the number at which the derived allele is carried only by samples n and y . We assume for the moment that we have no sample from the second archaic population, D . It contributes DNA to our sample only via gene flow into population Y . Thus, we have three I statistics: I_{ny} , I_{nx} , and I_{xy} . These definitions are summarized in table 1. If either archaic population contributed genes to population Y , then I_{ny} should exceed I_{nx} . This is indeed the case for the data summarized in table 1. Our goal is to use such discrepancies to study the rates, m_N and m_D , of gene flow from archaics into population Y .

2.3. Expectations of ratios

All the estimators discussed here use a ratio of expectations to approximate the expectation of a ratio. In each case, numerator and denominator are sums across all polymorphic sites in the sample. If the number of such sites is large, the weak law of large numbers implies that numerator and denominator should each be close to their expectations, so that the ratio of expectations is a good approximation. This approximation is quite accurate when samples are entire genomes. It would be less accurate in smaller regions, such as individual genes.

2.4. Time parameters

Greek letters represent time parameters, as summarized in table 3. The values there are in kiloyears (ky). Where possible, these are estimates taken from the literature, but we have not included statistical uncertainties because of our focus in this article on expected values and bias. Where published values are ranges, we use the midpoints. The parameters α and α' are intended bracket the time of gene flow from Denisovans into Eurasian populations. Although there are no compelling estimates of these parameters, it seems unlikely that this gene flow could have occurred much before 50 ky ago or much after 25 ky ago.

In calculations, the values in table 3 are re-expressed in units of $2N_0$ generations, where the generation time is 25 years, and $N_0 = 2308$ is the estimated size of the ancestral human population, as shown in table 2.

2.5. Simulations to validate theory

To check for errors in algebraic formulas, we developed software to simulate the components of each estimator. These simulations generate gene genealogies by running a coalescent process constrained by assumptions involving the population tree (branch lengths as well as topology), admixture events (timing as well as level of gene flow), and the size of each population. For details, see section ?? of *Supplementary Materials*.

3. Results

3.1. The estimator \hat{f} of Patterson and Reich (2010)

The first estimator to use the idea outlined in section 2.2 was that of Patterson and Reich (2010, Eqn. S18.5). Their estimator \hat{f} is designed to estimate Neanderthal gene flow. It can be written as

$$\hat{f} = \frac{I_{ny} - I_{nx}}{J_{n'n} - J_{nx}} \quad (1)$$

where n and n' are two genomes sampled from the Neanderthal population N . The numerator and denominator analyze different sets of genomes: $\{n, x, y\}$ and $\{n, n', x\}$. Because these sets differ, the number of sites with pattern nx will not in general be identical in the numerator and denominator. For this reason, we use J s rather than I s to represent counts of sites in the denominator.

In practice, Patterson and Reich (2010, p. 159) use a weighted average of two such estimators, in which the roles of the two Neanderthal fossils are switched. This does not change expected values, so we use the simpler formulation in Eqn. 1.

Appendix B derives the expected value of \hat{f} under a generalized model (Fig. 2), which allows for ghost admixture from archaic population D . The expected value is

$$E[\hat{f}] \approx \frac{m_N(1 - m_D)(\lambda - \delta + s_1) + m_D(\lambda - \kappa + s_2)}{(1 - m'_D)(\lambda - \varepsilon + s_3) + m'_D(\lambda - \kappa + s_2)} \quad (2a)$$

$$\approx m_N \left(\frac{\lambda - \delta + s_1}{\lambda - \varepsilon + s_3} \right) + m_D \left(\frac{\lambda - \kappa + s_2}{\lambda - \varepsilon + s_3} \right) \quad (2b)$$

where m_D and m'_D are rates of gene flow from D into Y and into N , and (2b) ignores 2nd-order terms in m_N , m_D , and m'_D . The s_i terms are

$$\begin{aligned} s_1 &= (1 - K_N)F_N^{(\delta, \kappa)} + (1 - K_{ND})S_N^{(\delta, \kappa)}F_{ND}^{(\kappa, \lambda)} \\ s_2 &= (1 - K_{ND})F_{ND}^{(\kappa, \lambda)} \\ s_3 &= (1 - K_N)F_N^{(\delta, \kappa)} + (1 - K_{ND})S_N^{(\varepsilon, \kappa)}F_{ND}^{(\kappa, \lambda)} \end{aligned}$$

and measure population-size bias. If all populations are of equal size, $s_i = 0$ for all i .

The expression $(1 - K_N)F_N^{(\delta, \kappa)}$, which appears in s_1 and s_3 , accounts for any difference in size between the ancestral

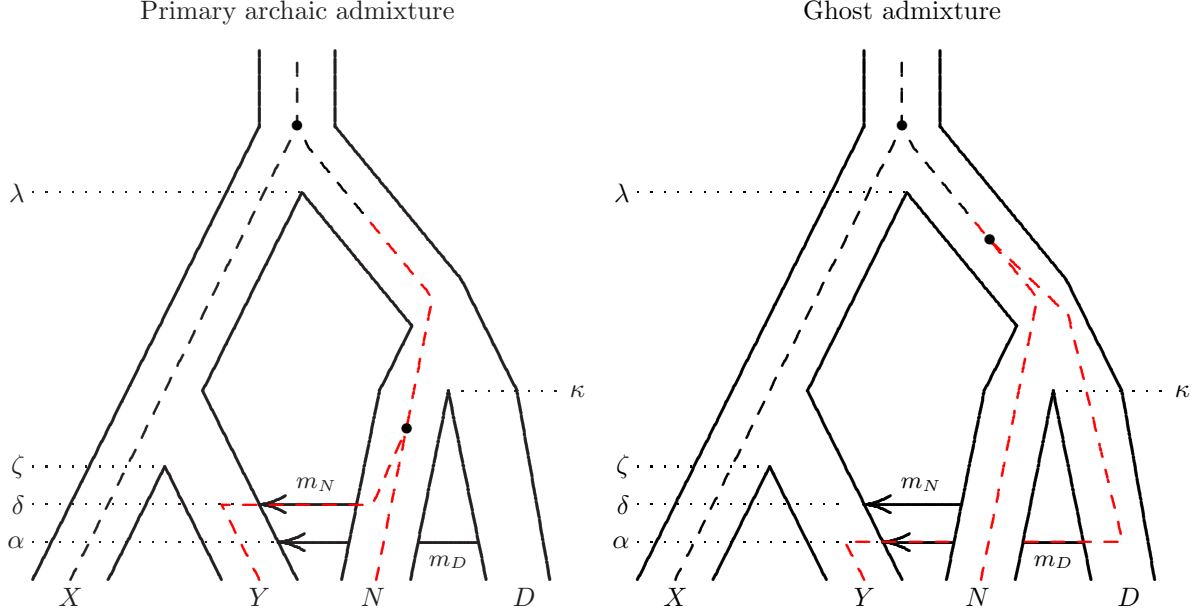


Figure 2: A population tree (solid lines) with embedded gene trees (dashed lines). In a sample from population Y , a fraction m_D of nucleotide sites descend from archaic population D . Of the remaining fraction $1 - m_D$, a fraction m_N descend via gene flow from archaic population N . Greek letters indicate time variables, as explained in table 3. Bullets delineate branches along which mutation would generate site pattern ny . Red indicates portion of genealogy carrying derived allele. Left panel: nucleotide sampled from Y comes from N and coalesces during (δ, λ) within population ND . Right panel: nucleotide sampled from Y comes from D and coalesces during (κ, λ) .

Table 3: Symbols and reference values for time parameters

Symbol	Value (ky)	Definition	Reference
α	25	latest plausible Denisovan admixture	a guess
α'	50	earliest plausible Denisovan admixture	a guess
β	40	separation time of Melanesians and other Eurasian populations	
ι	39.7	age of Mezmaiskaya fossil	(Pinhasi et al., 2011)
γ	40	age of Denisovan fossil	(Reich et al., 2010, p. 1053)
δ	55	time of Neanderthal admixture	(Sankararaman et al., 2012, table 2)
ε	65	age of older Neanderthal fossil used in \hat{f} or of Altai Neanderthal	(Green et al., 2010, pp. 713; Prüfer et al., 2014, table 1)
θ	95	separation time of populations of Mezmaiskaya and Altai Neanderthals	(Prüfer et al., 2014, p. 44)
ζ	110	separation time of Africans and Eurasians	(Veeramah and Hammer, 2014, p. 153)
η	200	separation time of San and other modern human populations	
κ	427	separation time of Neanderthal and Denisovan populations	(Prüfer et al., 2014, p. 44)
λ	658	separation time of modern and archaic populations	(Prüfer et al., 2014, p. 44)
μ		separation time of chimpanzee and hominin populations	

human population and N , the Neanderthal population. If N were small, a pair lineages would tend to coalesce within it, so $F_N^{(\delta, \kappa)}$ would be large. In addition, the early coalescence would lengthen the branch along which mutations can generate site pattern ny . The factor $1 - K_N$ accounts for this change in branch length, as explained in Appendix A.3. Taken together, these effects make s_1 and s_3 decreasing functions of K_N .

Eqn. 2b shows that \hat{f} estimates m_N , but not without bias. The bias disappears only if ghost admixture is absent ($m_D = 0$), population sizes are equal ($s_i = 0$), and the older fossil lived at the time of the gene flow from N into Y ($\delta = \varepsilon$). If the first two of these conditions hold, Eqn. 2b is equivalent to the result of Patterson et al. (2010b, p. 55). We consider the magnitudes of these biases below.

3.2. The estimator R_N of Patterson et al. (2010b)

Another method was needed for studying Denisovan admixture, because only one Denisovan genome is available. Patterson et al. (2010b) introduce two new statistics. The first of these, $R_{\text{Neanderthal}}$ (their Eqn. S8.3), estimates gene flow from Neanderthals. Patterson et al. (2012a, p. 42) call this statistic “Nea.” They also define an analogous statistic, “Den,” in which the roles of Neanderthal and Denisovan samples are reversed, and the goal is to estimate Denisovan admixture. The analysis for these statistics is the same, assuming that the Neanderthal and Denisovan populations are sister taxa within the population tree.

We abbreviate $R_{\text{Neanderthal}}$ as R_N and define it as

$$R_N = \frac{I_{de} - I_{ad}}{J_{dn} - J_{ad}} \quad (3)$$

In this statistic, the numerator compares an African genome, a , a Eurasian genome, e , and the Denisovan genome, d . A chimpanzee genome is used to infer the ancestral state. The denominator drops the Eurasian genome and adds a Neanderthal genome, n . These genomes are sampled from populations A , E , N , D , and C , using the model in Fig. 3.

We consider a model in which the Eurasian population received gene flow first from Neanderthals, at time δ , and then from Denisovans, at time α . The first of these episodes replaced a fraction m_N of the Eurasian gene pool; the second replaced a fraction m_D . The goal is to estimate Neanderthal gene flow, so m_D measures ghost admixture.

Appendix C derives the expectation of R_N ,

$$E[R_N] \approx m_N(1 - m_D) + m_D \left(\frac{\lambda - \alpha + s_4}{\lambda - \kappa + s_5} \right) \quad (4)$$

The s_i terms are

$$\begin{aligned} s_4 &= (1 - K_D)F_D^{(\alpha, \kappa)} + (1 - K_{ND})S_D^{(\alpha, \kappa)}F_{ND}^{(\kappa, \lambda)} \\ s_5 &= (1 - K_{ND})F_{ND}^{(\kappa, \lambda)} \end{aligned}$$

and measure population-size bias. If ghost admixture is absent ($m_D = 0$), then R_N provides an unbiased estimate of m_N (Patterson et al., 2010b, Eqn. S8.4; Durand and Slatkin, 2010, S11.9). Otherwise, it is affected by all three forms of bias. Fig. 4 shows how it varies in response to κ , the Neanderthal-Denisovan separation time.

3.3. The estimator R_D of Patterson et al. (2010b)

Patterson et al. (2010b, Eqn. S8.5) also define a second statistic, R_{Denisova} , which we abbreviate as R_D . It can be written as

$$R_D = \frac{I_{es} - I_{sv}}{J_{sy} - J_{ds}} \quad (5)$$

The numerator compares genomes sampled from three populations: San, S , Eurasian, E , and Melanesian, V . The chimpanzee, C , determines ancestral state. The denominator drops E and V but adds Yoruban, Y , and Denisovan, D . These populations are related as in Fig. 5. This model assumes that the ancestral Eurasian population exchanged a fraction m_N of its genes with Neanderthals. Later, the Melanesian population exchanged a fraction m_D with Denisovans. The goal is to estimate m_D , so m_N measures ghost admixture.

Appendix D derives an approximation to the expected value of R_D ,

$$E[R_D] \approx m_D(1 - m_N) \quad (6)$$

in agreement with published results (Patterson et al., 2010b, Eqn. S8.6; Durand and Slatkin, 2010, S11.19). Of the estimators considered here, this is the only one unaffected by bias involving branch lengths and changes in population size. It is sensitive to ghost admixture (m_N), but only slightly unless m_N is large. In an effort to remove this bias, Patterson et al. (2010b, p. 57) estimate m_D as $R_D/(1 - R_N)$. This involves using R_N with a population that received Denisovan gene flow. Because R_N is biased in such cases, this procedure imports bias into the estimate of m_D . This effect will be small, however, unless R_N is large.

3.4. The estimator p_D of Reich et al. (2011)

Patterson et al. (2012b, p. 1072) define a family of related statistics, which they call “ F_4 -ratio estimators.” Reich et al. (2011, Eqn. 1) use one of these to study how Denisovan admixture varies from population to population:

$$p_D = \frac{\sum_i (w_i - d_i)(x_i - y_i)}{\sum_i (w_i - d_i)(x_i - y'_i)} \quad (7)$$

In this equation, lower-case letters do not represent individual genomes. Instead, w_i , x_i , y_i , and d_i are frequencies of a given allele at locus i within four populations, W , X , Y , and D . In the denominator, y'_i is the frequency within a fifth population, Y' . The model assumes that Y' occupies a position within the population tree that is similar to that of Y . In other words, the tree of W , X , Y' , and D is identical to that in figure 6. The goal is to estimate the ratio m_D/m'_D of Denisovans admixture into Y and Y' . The

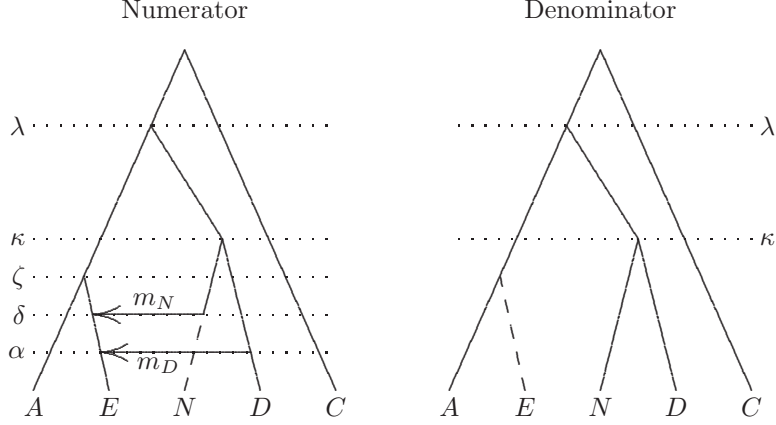


Figure 3: Population tree for R_N (Patterson et al., 2010b, Eqn. S8.3). The populations involved are Africa (A), Eurasia (E), Neanderthal (N), Denisova (D), and chimpanzee (C). Arrows indicate gene flow from Neanderthals at rate m_N and, later, from Denisovans at rate m_D . Only four populations are compared in the numerator of R_N , and a different four are compared in the denominator. In each panel of the figure, dashed line indicates the sample being ignored. Greek letters represent the times of various events.

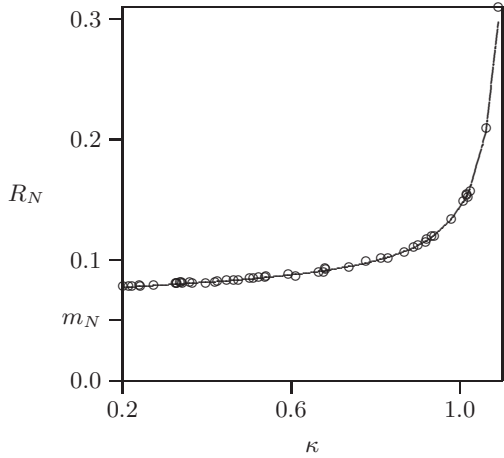


Figure 4: Response of R_N to the separation time, κ , of Neanderthals and Denisovans. Circles show simulated values and solid line shows theoretical formula (Eqn. 4). Simulations generate branch lengths only (not mutations) and are described in section 2.5. They use 10^6 iterations, assume $m_N = 0.05$, $m_D = 0.025$, and other parameters as in tables 2–3. κ is in units of $2N_0$ generations.

corresponding Neanderthal rates, m_N and m'_N , measure ghost admixture.

Appendix E derives the expected value of p_D under a mutational clock. This is a departure from Reich et al. (2011), who couch their theory in terms of genetic drift. Although Reich et al. define w_i , x_i , y_i , and d_i as frequencies of an arbitrary allele, these become derived allele frequencies in our analysis. We drop the assumption (Patterson et al., 2012b, p. 1069) that the locus is polymorphic at the root of the human tree. The expected value of p_D is approximately

$$E[p_D] \approx \frac{m_D A + m_N (1 - m_D) B}{m'_D A' + m'_N (1 - m'_D) B} \quad (8)$$

where

$$A = 2\lambda - \zeta - \alpha + s_6$$

$$A' = 2\lambda - \zeta - \alpha' + s_7$$

$$B = 2\lambda - \zeta - \kappa + s_8$$

and α and α' are the times of Denisovan gene flow into populations Y and Y' . The s_i ,

$$s_6 = 2T_0^{(\lambda)} - T_{WXY}^{(\zeta)} - T_D^{(\alpha)}$$

$$s_7 = 2T_0^{(\lambda)} - T_{WXY}^{(\zeta)} - T_D^{(\alpha')}$$

$$s_8 = 2T_0^{(\lambda)} - T_{WXY}^{(\zeta)} - T_{ND}^{(\kappa)}$$

measure population-size bias and disappear under constant size.

If population size is constant, Neanderthal admixture is absent, and the two Denisovan admixtures were simultaneous, then our results reduce to $E[p_D] = m_D/m'_D$, in agreement with Reich et al. (2011, p. 523).

3.5. The estimator p_N

Patterson et al. (2014, Eqn. S14.13) use another F_4 -ratio statistic to estimate the level of Neanderthal admixture into Europeans. Although they refer to it as $\hat{\alpha}$, we

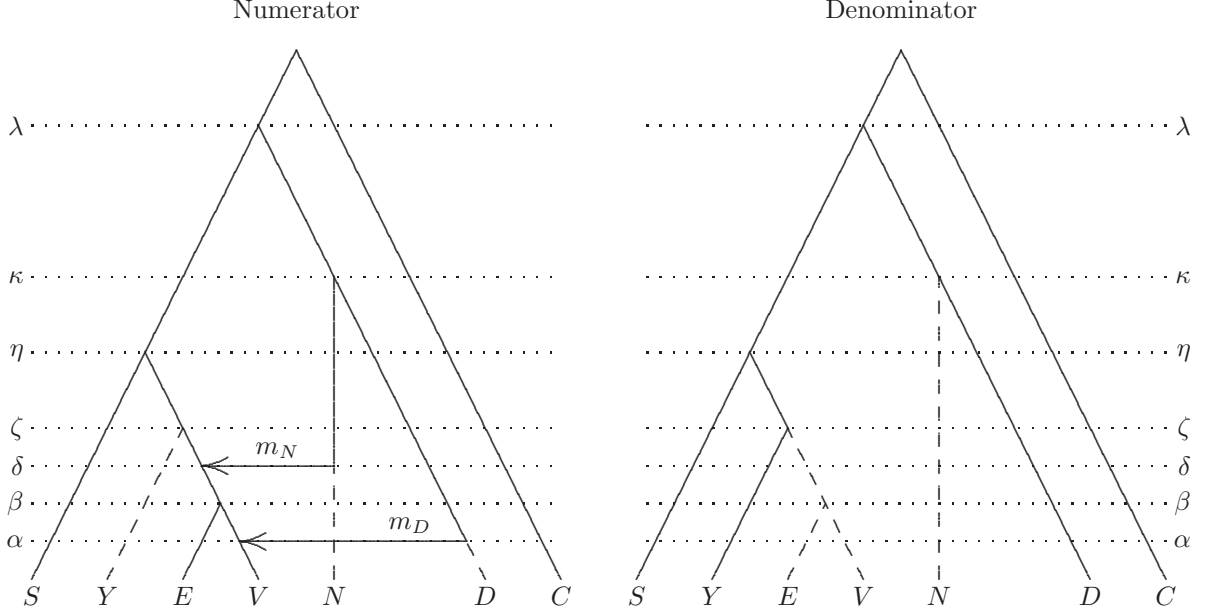


Figure 5: Population tree for R_D (Patterson et al., 2010b, Eqn. S8.5). The populations involved are San (S), Yoruba (Y), Eurasia (E), Melanesia (V), Neanderthal (N), Denisova (D), and chimpanzee (C). Arrows indicate gene flow from Neanderthals, at rate m_N , and Denisovans, at rate m_D . Although seven populations are involved, only four are compared in the numerator of R_D , and a different four are compared in the denominator. In each panel of the figure, dashed lines indicate the samples being ignored. Greek letters represent the times of various events.

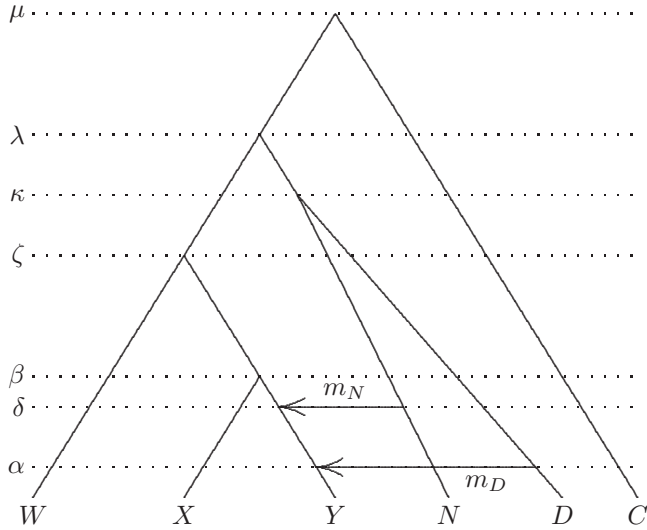


Figure 6: Population tree for p_D . W , X , and Y are three modern human populations; N and D are two archaic populations, and C is the chimpanzee population. A fraction m_D of the gene pool of Y descends via gene flow from D . Of the remaining fraction $1 - m_D$, a fraction m_N descends via gene flow from N . Greek letters represent the times of various events.

refer to it as p_N to avoid confusion with the time parameter, α , defined in our table 3. It is defined as

$$p_N = \frac{\sum_i (d_i - n_i)(a_i - x_i)}{\sum_i (d_i - n_i)(a_i - m_i)} \quad (9)$$

As with p_D , the lower-case letters represent not haploid genomes, but allele frequencies within four populations, which are related as shown in Fig. 7. We generalize the model of Patterson et al. to allow for ghost admixture (from Denisovans) as well as primary admixture (from Neanderthals).

We analyze this statistic under a molecular clock. The expectation of p_N , as derived in Appendix F, is

$$E[p_N] \approx m_N(1 - m_D) - m_D \left(\frac{\kappa - \alpha + s_9}{\kappa - \theta + s_{10}} \right) \quad (10)$$

where the terms

$$s_9 = T_{IMND}^{(\kappa)} - T_D^{(\alpha)}, \quad \text{and} \\ s_{10} = T_{IMND}^{(\kappa)} - T_{IMN}^{(\theta)}$$

measure population-size bias. In the absence of ghost admixture, $m_D = 0$, and $E[p_N] \approx m_N$, in agreement with Patterson et al. (2014, Eqn. S14.2). In this case, p_N is unbiased.

When ghost admixture is present, however, substantial biases arise. The interval $(\kappa - \alpha)$ in the numerator extends from the Neanderthal-Denisovan separation to the admixture of Denisovans into moderns. Although this interval is not well constrained, it must have been hundreds of

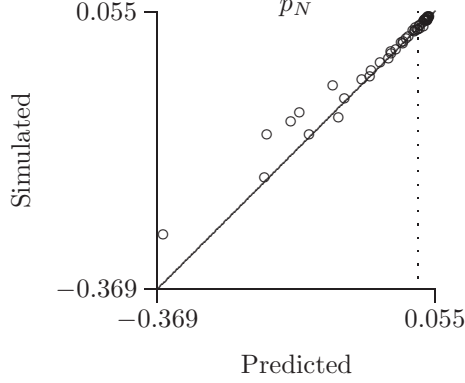


Figure 7: Population tree for p_N . A is the modern African population, X is a modern admixed population, I is the introgressing Neanderthal population, M is the population of the Mezmaiskaya Neanderthal, N that of the Altai Neanderthal, D is Denisova, and C is chimpanzee. A fraction m_D of the gene pool of X descends via gene flow from D . Of the remaining fraction $1 - m_D$, a fraction m_N descends via gene flow from I . Greek letters represent the times of various events.

thousands of years. The interval $(\kappa - \theta)$ in the denominator extends from the Neanderthal-Denisovan separation to that of the populations of the Mezmaiskaya and Altai Neanderthals and is probably much shorter. This suggests that, in Eqn. 10, the coefficient of m_D may exceed that of m_N . If so, p_N is more sensitive to ghost admixture than to primary admixture.

The coefficient of m_D also includes terms involving changes in population size. Although p_N is unbiased in the absence of ghost admixture, it is affected by all three forms of bias when ghost admixture is present.

3.6. A new estimator

Let us revisit the history illustrated in Fig. 2, whose properties are studied in Appendix B. We propose to estimate m_N with the ratio

$$Q = \frac{I_{ny} - I_{nx}}{I_{xy} - I_{nx}} \quad (11)$$

Unlike most of those published previously, this statistic requires only one archaic genome. The expectation of Q is approximately the ratio of Eqns. B.12a and B.12b,

$$E[Q] \approx \frac{m_N(1 - m_D)(\lambda - \delta + s_1) + m_D(\lambda - \kappa + s_2)}{(1 - m_N)(1 - m_D)(\lambda - \zeta + s_{11})} \quad (12a)$$

$$\approx m_N \left(\frac{\lambda - \delta + s_1}{\lambda - \zeta + s_{11}} \right) + m_D \left(\frac{\lambda - \kappa + s_2}{\lambda - \zeta + s_{11}} \right) \quad (12b)$$

where s_1 and s_2 are as defined in section 3.1, and

$$s_{11} = (1 - K_{XY})F_{XY}^{(\zeta, \lambda)}$$

Q is sensitive to all three forms of bias but is especially sensitive to population-size differences. Recent estimates indicate that archaic populations were much smaller than

Table 4: Elasticities of \hat{f} , R_N , p_D , p_N , and Q with respect to times and population sizes. The table assumes a level, 0.05, of primary admixture and 0.025 of ghost admixture, and other parameters as in tables 2–3. For p_D , we assume that $m_D = 0.1$ and $m'_D = 0.05$. Elasticities with absolute values greater than 0.5 are in bold type.

	\hat{f}	R_N	p_D	p_N	Q
λ	0.187	-0.623	-0.081		-0.247
κ	-0.241	0.724	0.063	0.364	-0.257
δ	-0.065				-0.065
θ				-0.438	
ε	0.095				
ζ			0.006		0.237
α		-0.019		-0.101	
α'			0.033		
K_N	0.008				-0.034
K_D		-0.022	0.004	0.093	
K_{ND}	-0.016	0.049	0.004		-0.017
K_{IMND}				-0.006	
K_{IMN}				-0.097	
K_{XY}					0.415
K_{WXY}			0.054		

early modern ones (Prüfer et al., 2014, Fig. 4). This makes s_1 and s_2 larger than s_{11} and biases Q upwards. Branch lengths provide an additional upward bias, because $\lambda - \delta$ probably exceeds $\lambda - \zeta$.

3.7. Effects of branch lengths and population sizes

To get a sense of magnitudes, let us calculate the expected value of each statistic under standard assumptions. We use the parameter values in tables 2–3, take the level of primary admixture as 0.05 and that of secondary admixture as 0.025. For p_D , we set $m_D = 0.1$ in the numerator and $m'_D = 0.05$ in the denominator. With these values,

$$\left. \begin{aligned} E[\hat{f}] &\approx 1.24 \times m_N \\ E[R_N] &\approx 2.11 \times m_N \\ E[R_D] &\approx 0.98 \times m_D \\ E[p_D] &\approx 0.89 \times m_D/m'_D \\ E[p_N] &\approx 0.37 \times m_N \\ E[Q] &\approx 1.92 \times m_N/(1 - m_N) \end{aligned} \right\} \quad (13)$$

These should not be viewed as precise numerical estimates of bias. Instead, they are representative values under one set of parameter values. Under these assumptions, the estimators differ greatly in bias. The multiplier for R_D is close to unity, indicating that it is nearly unbiased. The other estimators have substantial biases.

These biases could be corrected, given branch lengths, population sizes and the rate of ghost admixture, by equating observed to expected values and solving for primary admixture. The trouble is that these parameters cannot be estimated precisely, and any error would bleed into estimates of admixture. To measure sensitivity to these uncertainties, we calculate *elasticities*.

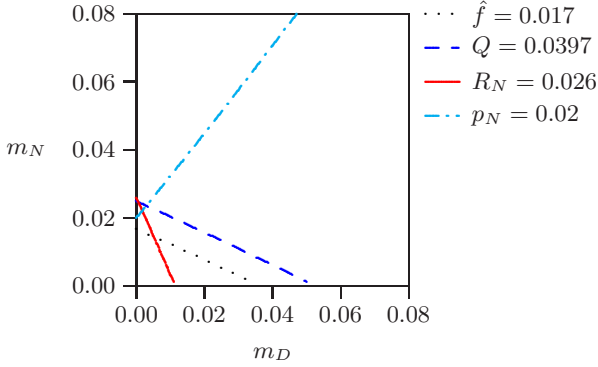


Figure 8: Archaic admixture in France, as implied by estimates of \hat{f} (Patterson and Reich, 2010, table S58), Q (this article), R_N (Patterson et al., 2010b, p. 55), and p_N (Patterson et al., 2014, p. 128). Curves assume values in tables 2–3.

Elasticity is the proportional change in one quantity caused by a given proportional change in another. For example, the elasticity of \hat{f} with respect to λ is $d \log E[\hat{f}] / d \log \lambda$. R_D has elasticity zero with respect to branch lengths and population sizes. The elasticities of the other statistics are shown in table 4, evaluated at the values in tables 2–3. Elasticities larger than 0.5 are shown in bold. The elasticity with largest absolute value, 0.724, is that of R_N with respect to κ . If the true value of κ were 10% larger than our estimate, R_N would be inflated by about 7%. Fig. 4 shows this response in greater detail.

The relatively large elasticities of R_N , p_N , and Q make them sensitive to error in parameter estimates. The outlook is brighter for \hat{f} , p_D , and R_D , which have smaller elasticities.

3.8. Effect of ghost admixture

Each statistic is designed to estimate admixture from a specific archaic population. We refer to this as “primary admixture.” However, the expected values of these statistics also depend on “ghost” admixture from other archaic populations.

To see this effect, consider the statistic Q . Substituting from table 1 into Eqn. 11 gives

$$Q = \frac{103,612 - 95,347}{303,340 - 95,347} \approx 0.0397$$

After setting $Q = E[Q]$, Eqn. 12 defines m_N as an implicit function of m_D . This function is shown as a dark blue dashed line in Fig. 8. The slope of that line measures the sensitivity of Q to ghost admixture. If ghost admixture is absent, this estimate suggests that a fraction $m_N = 0.025$ of French DNA derives from Neanderthals. This estimate does not equal Q , because it corrects for bias using the parameter values in tables 2–3. If ghost admixture were 5%, on the other hand, we would conclude that $m_N = 0$. By itself, Q cannot choose between these alternatives.

This ambiguity evaporates when we consider other estimators. The other curves in Fig. 8 refer to other statistics

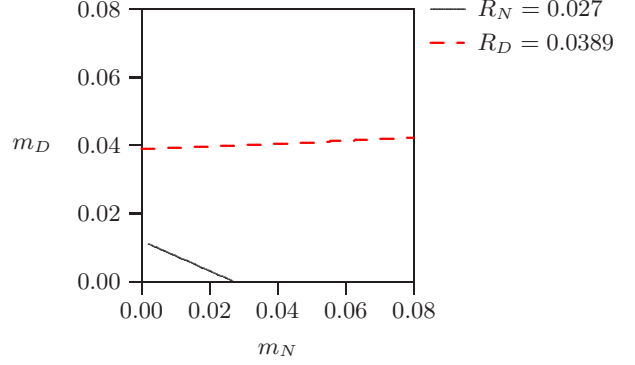


Figure 9: Archaic admixture in Melanesia, as implied by the observation that $R_N = 0.027$ and $R_D/(1 - R_N) = 0.04$ (Patterson et al., 2010b, p. 58). Curves assume values in tables 2–3.

that have been used to estimate Neanderthal admixture into the French population. The curves have very different slopes, because the estimators respond differently to ghost admixture. In the absence of sampling error and uncertainty about parameter values, they should all intersect at a point corresponding to the true values of m_N and m_D . Although the curves do not intersect at a point, the difference between them is smallest near the left edge of the graph, where m_D is small. This suggests that the French received archaic gene flow primarily from Neanderthals, in agreement with Reich et al. (2010, p. 1056).

The agreement between Q and the other statistics also tells us something about ancient population sizes. As table 4 shows, Q is sensitive to population sizes. Indeed, if one builds a graph like Fig. 8 *without* correcting for population size, Q is not consistent with the other estimators (data not shown). In correcting for population size, we have assumed that archaic populations were much smaller than early modern ones, as shown in table 2. Had this assumption been incorrect, the correction would not have helped. Thus, the consistency between Q and the other estimators supports current views about the sizes of ancient populations (Meyer et al., 2012, Fig. 5; Prüfer et al., 2014, Fig. 4).

Fig. 9 attempts a similar analysis with Melanesian data. For that population, Patterson et al. (2010b, p. 58) estimate that $R_N = 0.027$ and $R_D/(1 - R_N) = 0.04$, which implies that $R_D = 0.0389$. At face value, these data suggest that the Melanesian gene pool includes a small contribution from Neanderthals and a larger one from Denisovans. The curves in Fig. 9, however, do not support this view. The two curves are far apart throughout the horizontal range. Even if Melanesians received no Neanderthal admixture at all, R_N should be much higher than the observed value.

There are several conceivable explanations for this discrepancy. First, it could result from sampling error in the estimates of R_N and R_D . This seems unlikely, in view of the large sample of sites, but cannot be excluded without statistical analysis. We do not attempt such an analysis here. Second, the discrepancy could result from error in

the parameter values in tables 2–3. It would be useful to fit these parameters rather than taking their values as given. Finally, the discrepancy could arise because the model is misspecified—because the history of the populations under study violates the assumptions in Figs. 3 and 5. We discuss this last possibility below.

4. Discussion and Conclusions

This article has explored biases that arise in one family of estimators—those based on the frequency with which derived alleles are shared by pairs of samples. We have focused on three forms of bias, involving branch lengths in the population tree, differences in population size, and ghost admixture.

All of these estimators are sensitive to “ghost admixture”—to admixture from archaic populations other than the one of primary interest. The most robust estimator, R_D , is hardly affected. The others are at least modestly sensitive. For R_N and p_N , this effect is profound.

Branch-length bias arises because the effect of admixture depends not only on the number of immigrants, but also on the genetic difference between immigrants and residents. The longer the two populations have been separated, the greater their genetic difference, and the greater the effect of any given level of gene flow. For this reason, the expected values of admixture statistics may depend on branch lengths.

Yet in the absence of ghost admixture, most published estimators are relatively free of branch-length bias. Each is constructed as a ratio. When branch length effects are identical in numerator and denominator, they cancel, and the resulting expression is free of branch-length bias. This cancellation often fails, however, in the presence of ghost admixture. In that case, there may be two branch-length effects, which cannot both cancel in a single ratio. For this reason, branch lengths bias R_N and p_N only in the presence of ghost admixture. With other estimators, branch lengths contribute bias even in the absence of ghost admixture. Only R_D escapes this effect.

Where branch-length effects exist, they are accompanied by terms involving differences in population size. These differences distort branch lengths within the gene genealogy and thus alter the probability that mutations will generate particular site patterns. These effects, however, are generally small, at least for the parameter values in tables 2–3. Population-size bias is substantial only for the new estimator, Q .

The estimators respond to ghost admixture in different ways, as shown by their differing slopes in Figs. 8 and 9. Because of these differences, comparisons among estimators provide information. Such comparisons indicate that archaic gene flow into Europe came primarily from Neanderthals and support the view that archaic populations were much smaller than those of early modern humans.

They also expose an inconsistency in estimates of archaic admixture into Melanesia. As shown in Fig. 9, no pair of (m_N, m_D) values is consistent both with the observed value of R_N and also with that of R_D .

Although this inconsistency may be a statistical artifact, it could also result from an incorrectly specified model. For example, *Homo erectus* may have contributed genes to populations of Denisovans (Prüfer et al., 2014, p. 48) or to modern humans in Melanesia (Mendez et al., 2012). Such gene flow would violate the assumptions underlying our analysis of R_N and R_D and might account for the discrepancy seen in Fig. 9.

Our empirical conclusions should be regarded with caution, because we have made no effort to account for statistical uncertainty. Nonetheless, the exercise illustrates that the biases in these estimators are not altogether bad. Because these estimators respond to population history in different ways, comparisons among them provide new information.

Appendix A. Probabilities of site patterns

Within a tree of populations, many different gene trees are possible. For example, Fig. A.10 illustrates two ways in which the gene tree of lineages x_1 , x_2 , and z can coalesce within the same population tree. On the left, x_1 and x_2 coalesce during the interval (t_0, t_1) within population X . On the right, no coalescent event occurs during this interval. Instead, the first coalescent event occurs prior to time t_2 , within the ancestral population, XYZ .

When the coalescent event occurs within (t_0, t_1) , only one site pattern can be produced: x_1x_2 . But if it occurs earlier, before time t_2 , all three site patterns are equally likely. For this reason, it is necessary to distinguish these cases when calculating the probabilities of site patterns. Our analysis uses the method of Durand et al. (2010), Durand and Slatkin (2010), and Durand et al. (2011). This section explains the general principles.

Appendix A.1. Expectation of a truncated exponential random variable

Let t represent an exponential random variable with mean K . We are interested in the conditional expectation of t , given that t is less than an arbitrary value, z . The mean can be written as

$$K = F^{(0,z)}E[t|t < z] + S^{(0,z)}E[t|t > z]$$

Where $S^{(0,z)} = e^{-z/K}$ is the probability that $t > z$, and $F^{(0,z)} = 1 - S^{(0,z)}$ is the probability that $t < z$. The memoryless property of the exponential distribution implies that $E[t|t > z] = z + K$. Substituting and rearranging,

$$E[t|t < z] = K - zS^{(0,z)}/F^{(0,z)}, \quad (\text{A.1})$$

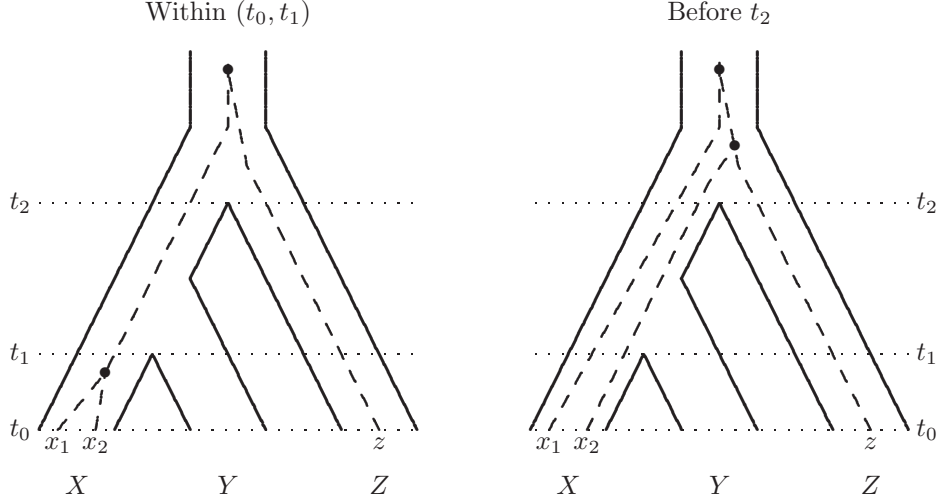


Figure A.10: Coalescent events within an interval (left panel) and in the ancestral population (right panel). During interval (t_0, t_1) , a coalescent event can occur only between lineages x_1 and x_1 . The left panel illustrates this case. Prior to time t_2 , coalescent events can occur between any pair of lineages. The right panel illustrates the case in which x_2 and z coalesce first. Bullets delineate the branches along which mutation would generate site pattern x_1x_2 (left panel) or x_2z (right panel).

Appendix A.2. Coalescent waiting time under piecewise constant hazard

Suppose that population history is a sequence of epochs, numbered backwards from the present. The i th epoch spans the interval (t_i, t_{i+1}) , where time is measured backwards from the present. Within the i th epoch, the diploid population size (relative to N_0) is a constant, K_i . For a single pair of lineages within interval i , the hazard of a coalescent event is $1/K_i$ per coalescent time unit.

Consider a pair of lineages at time x , which lies within epoch i . In other words, $t_i < x < t_{i+1}$. We are interested in the expected time, $T_i^{(x)}$, until they coalesce. Either they coalesce within epoch i (with probability $F_i^{(x, t_{i+1})}$), or they survive into epoch $i+1$ (with probability $S_i^{(x, t_{i+1})}$). In the former case, the expected coalescence time is given by Eqn. A.1. In the latter, it is $t_{i+1} - x + T_{i+1}^{(t_{i+1})}$. This leads to

$$T_i^{(x)} = K_i + S_i^{(x, t_{i+1})}(T_{i+1}^{(t_{i+1})} - K_i) \quad (\text{A.2})$$

We assume the final epoch is infinite. This implies that $T_j^{(x)} = K_j$, if j is the final epoch. For other epochs, Eqn. A.2 can be applied recursively to calculate $T_i^{(x)}$. If population size is constant, $K_i = T_i^{(x)} = 1$ for all i .

If epoch j represents the ancestral human population, then $K_j = 1$, as explained in section 2.1. We will often assume, in addition, that $T_j^{(x)} = 1$ in this population. This amounts to assuming that no changes in population size occurred prior to the ancestral human population. In the analyses of p_D and p_N , however, we extend the model farther back in time to include the population ancestral to chimpanzees and humans.

Appendix A.3. Coalescent event within an interval

Consider the left panel of Fig. A.10, in which lineages x_1 and x_2 coalesce during (t_0, t_1) , within population X . This occurs with probability $P = F_X^{(t_0, t_1)}$, as explained in section 2.1. In this case, the gene tree will be of form $((x_1, x_2), z)$, as required by site pattern x_1x_2 . But even when this genealogy does arise, we cannot be sure that site pattern x_1x_2 will appear in the data. That happens only when a mutation falls on the branch delineated by bullets in the left panel of Fig. A.10.

The probability of such a mutation depends on branch lengths. Let w represent the time, within interval (t_0, t_1) , at which the coalescent event occurs. In other words, the event occurs at time $t_0 + w$, measuring time backwards from the present. The expectation of w is given by Eqn. A.1.

Continuing into the past, we can trace the single lineage ancestral to x_1 and x_2 . At time t_2 , it becomes part of population XYZ . After an additional v units of time, it coalesces with lineage z . Here, v is the coalescence time within population XYZ and has mean $T_{XYZ}^{(t_2)}$, as explained in Appendix A.2.

Pattern x_1x_2 is generated when a mutation occurs on the branch that separates two coalescent events: one that joins x_1 and x_2 , and another that joins their common ancestor to lineage z . This branch is delineated by bullets in the left panel of Fig. A.10. Its length, $t_2 + v - t_0 - w$, has expectation

$$B = (t_1 - t_0)/F_X^{(t_0, t_1)} + t_2 - t_1 + T_{XYZ}^{(t_2)} - K_X$$

The probability that a mutation falls on this branch, producing site pattern x_1x_2 , is approximately UB , where U is the mutation rate defined in section 2.1.

Combining all this, we can calculate the probability that a coalescent event falls within interval (t_0, t_1) and

gives rise to a site with pattern x_1x_2 . The probability is the product of P (the probability of the appropriate genealogy) and UB (the probability of a mutation on the resulting branch). Altogether, this equals UPB , where

$$PB = t_1 - t_0 + (t_2 - t_1 + T_{XYZ}^{(t_2)} - K_X)F_X^{(t_0, t_1)}$$

In a population of constant size, $K_X = T_{XYZ}^{(t_2)} = 1$.

Appendix A.4. Coalescent event within the ancestral population

Consider now the case illustrated in the right panel of Fig. A.10. No coalescent event occurs during (t_0, t_2) —an event of probability $S_X^{(t_0, t_1)}S_{XY}^{(t_1, t_2)}$. Consequently, all three lineages enter the ancestral population, XYZ . These can coalesce in any order, so we are equally likely to see genealogies $((x_1, x_2), z)$, $((x_1, z), x_2)$, and $(x_1, (x_2, z))$. The probability of any given genealogy is $P = S_X^{(t_0, t_1)}S_{XY}^{(t_1, t_2)}/3$.

If the first pair of lineages coalesces at time $x > t_2$, the waiting time until the second coalescent event is $B = T_{XYZ}^{(x)}$, as explained in Appendix A.2. This case generates each of the three site patterns with probability UPB , where

$$PB = S_X^{(t_0, t_1)}S_{XY}^{(t_1, t_2)}T_{XYZ}^{(x)}/3$$

A similar result was derived by Hudson (1992, Eqn. 6).

If XYZ is the ancestral human population, we will usually assume that $T_{XYZ}^{(x)} = 1$, as discussed in Appendix A.2.

Appendix B. Expected value of \hat{f}

\hat{f} is defined in Eqn. 1 and assumes the population history in Fig. 2. The numerator of \hat{f} involves four genomes, x , y , n , and c , sampled from two populations, X and Y , of modern humans, one archaic population, N , and the chimpanzee population, C . The chimpanzee population is used only to determine which allele is derived and is not shown in Fig. 2. The Eurasian population received gene flow from Neanderthals at time δ and from Denisovans at a later time, α . The first of these episodes replaced a fraction m_N of the Eurasian gene pool; the second replaced a fraction m_D . The remaining fraction $(1 - m_N)(1 - m_D)$ is “native”—it derives from the population, XY , of ancestral modern humans.

1 y arrived by gene flow from D

- 1.1 y and n coalesce within ND , during (κ, λ) . Sites in this category contribute to pattern ny only. The argument in Appendix A.3 gives $P = m_DF_{ND}^{(\kappa, \lambda)}$; $B = (\lambda - \kappa)/F_{ND}^{(\kappa, \lambda)} + 1 - K_{ND}$; and

$$PB = m_D\{\lambda - \kappa + (1 - K_{ND})F_{ND}^{(\kappa, \lambda)}\} \quad (\text{B.1})$$

- 1.2 y and n coalesce in the ancestral human population. This case can give rise to any of the three

genealogies. The argument in Appendix A.4 gives $P = m_DS_{ND}^{(\kappa, \lambda)}/3$; $B = 1$; and

$$PB = m_DS_{ND}^{(\kappa, \lambda)}/3 \quad (\text{B.2})$$

2 y arrived by gene flow from N .

- 2.1 y and n coalesce within N , during (δ, κ) . Sites in this category contribute to pattern ny only. The argument in Appendix A.3 gives $P = m_N(1 - m_D)F_N^{(\delta, \kappa)}$; $B = \lambda - \kappa + 1 - K_N + (\kappa - \delta)/F_N^{(\delta, \kappa)}$; and

$$PB = m_N(1 - m_D)\{\kappa - \delta + (\lambda - \kappa + 1 - K_N)F_N^{(\delta, \kappa)}\} \quad (\text{B.3})$$

- 2.2 y and n coalesce within ND , during (κ, λ) . Contributes to pattern ny only. The argument in Appendix A.3 gives $P = m_N(1 - m_D)S_N^{(\delta, \kappa)}F_{ND}^{(\kappa, \lambda)}$; $B = 1 - K_{ND} + (\lambda - \kappa)/F_{ND}^{(\kappa, \lambda)}$; and

$$PB = m_N(1 - m_D)S_N^{(\delta, \kappa)}\{\lambda - \kappa + (1 - K_{ND})F_{ND}^{(\kappa, \lambda)}\} \quad (\text{B.4})$$

The total contribution from these last two cases is obtained by summing Eqns. B.3 and B.4:

$$PB = m_N(1 - m_D)\{\lambda - \delta + (1 - K_N)F_N^{(\delta, \kappa)} + (1 - K_{ND})S_N^{(\delta, \kappa)}F_{ND}^{(\kappa, \lambda)}\} \quad (\text{B.5})$$

- 2.3 y and n coalesce in the ancestral human population. Contributes to all three site patterns. The argument in Appendix A.4 gives $P = m_N(1 - m_D)S_N^{(\delta, \kappa)}S_{ND}^{(\kappa, \lambda)}/3$; $B = 1$; and

$$PB = m_N(1 - m_D)S_N^{(\delta, \kappa)}S_{ND}^{(\kappa, \lambda)}/3 \quad (\text{B.6})$$

3 y is native.

- 3.1 x and y coalesce in XY , during (ζ, λ) . Contributes to site pattern xy only. The argument in Appendix A.3 gives $P = (1 - m_N)(1 - m_D)F_{XY}^{(\zeta, \lambda)}$; $B = 1 - K_{XY} + (\lambda - \zeta)/F_{XY}^{(\zeta, \lambda)}$; and

$$PB = (1 - m_N)(1 - m_D)\{\lambda - \zeta + (1 - K_{XY})F_{XY}^{(\zeta, \lambda)}\} \quad (\text{B.7})$$

- 3.2 x and y coalesce in the ancestral human population prior to λ . Contributes to all three site patterns. The argument in Appendix A.4 gives $P = (1 - m_N)(1 - m_D)S_{XY}^{(\zeta, \lambda)}/3$; $B = 1$;

$$PB = (1 - m_N)(1 - m_D)S_{XY}^{(\zeta, \lambda)}/3 \quad (\text{B.8})$$

These results are summarized in table B.5.

In this table, the only rows that contribute to pattern nx are those that contribute to all three site patterns. The expected value of I_{nx} is the sum of these rows times the

Table B.5: Contributions to each site pattern for estimators \hat{f} and Q . Each row represents a different case—a different way in which coalescent events can be distributed within the population tree. P_i is the probability of each such case, and B_i is the conditionally expected length of the branch along which mutation would give rise to each site pattern. $P_i B_i$ is the contribution of the current case to the unconditionally expected branch length. “Source” is the population from which sample y derives. “Coal.” indicates the time interval containing the most recent coalescent event. “Ref” refers to equation numbers in Appendix B.

Source	Coal.	$P_i B_i$	Ref
<i>Site Pattern ny only</i>			
N	(δ, λ)	$m_N(1 - m_D)\{\lambda - \delta + (1 - K_N)F_N^{(\delta, \kappa)} + (1 - K_{ND})S_N^{(\delta, \kappa)}F_{ND}^{(\kappa, \lambda)}\}$	B.5
D	(κ, λ)	$m_D\{\lambda - \kappa + (1 - K_{ND})F_{ND}^{(\kappa, \lambda)}\}$	B.1
<i>Site Pattern xy only</i>			
XY	(ζ, λ)	$(1 - m_N)(1 - m_D)\{\lambda - \zeta + (1 - K_{XY})F_{XY}^{(\zeta, \lambda)}\}$	B.7
<i>All Three Site Patterns</i>			
N	$> \lambda$	$m_N(1 - m_D)S_N^{(\delta, \kappa)}S_{ND}^{(\kappa, \lambda)}/3$	B.6
D	$> \lambda$	$m_DS_{ND}^{(\kappa, \lambda)}/3$	B.2
XY	$> \lambda$	$(1 - m_N)(1 - m_D)S_{XY}^{(\zeta, \lambda)}/3$	B.8

product of U (the mutation rate per unit of coalescent time) and L (the number of nucleotide sites sampled):

$$E[I_{nx}] = \frac{UL}{3} \left[m_N(1 - m_D)S_N^{(\delta, \kappa)}S_{ND}^{(\kappa, \lambda)} + m_DS_{ND}^{(\kappa, \lambda)} + (1 - m_N)(1 - m_D)S_{XY}^{(\zeta, \lambda)} \right] \quad (\text{B.9})$$

These same rows also contribute to site pattern ny , along with several additional rows that contribute only to ny . Thus,

$$E[I_{ny}] = E[I_{nx}] + UL \left[m_N(1 - m_D)\{\lambda - \delta + (1 - K_N)F_N^{(\delta, \kappa)} + (1 - K_{ND})S_N^{(\delta, \kappa)}F_{ND}^{(\kappa, \lambda)}\} + m_D\{\lambda - \kappa + (1 - K_{ND})F_{ND}^{(\kappa, \lambda)}\} \right] \quad (\text{B.10})$$

Similarly,

$$E[I_{xy}] = E[I_{nx}] + UL(1 - m_N)(1 - m_D) \left[\lambda - \zeta + (1 - K_{XY})F_{XY}^{(\zeta, \lambda)} \right] \quad (\text{B.11})$$

Eqns. B.9–B.10 extend results derived by Durand et al. (2011, Eqns. 3–4).

The excesses of I_{ny} and I_{xy} over I_{nx} are

$$E[I_{ny} - I_{nx}] \propto m_N(1 - m_D)\{\lambda - \delta + (1 - K_N)F_N^{(\delta, \kappa)} + (1 - K_{ND})S_N^{(\delta, \kappa)}F_{ND}^{(\kappa, \lambda)}\} + m_D\{\lambda - \kappa + (1 - K_{ND})F_{ND}^{(\kappa, \lambda)}\} \quad (\text{B.12a})$$

$$E[I_{xy} - I_{nx}] \propto (1 - m_N)(1 - m_D)\{\lambda - \zeta + (1 - K_{XY})F_{XY}^{(\zeta, \lambda)}\} \quad (\text{B.12b})$$

omitting the constant multiplier, UL .

The analysis of the denominator is identical to that of the numerator, except that $m_N = 1$ (because samples n' and n are both from the same Neanderthal population),

and δ (the time of gene flow) is replaced by ε (the age of the older of the two archaic fossils) (Durand et al., 2010, p. 169). The symbol m'_D will represent the rate of Denisovan gene flow into Neanderthals. With these changes, Eqn. B.12a becomes

$$E[J_{n'n} - J_{nx}] \propto (1 - m'_D)\{\lambda - \varepsilon + (1 - K_N)F_N^{(\delta, \kappa)} + (1 - K_{ND})S_N^{(\varepsilon, \kappa)}F_{ND}^{(\kappa, \lambda)}\} + m'_D\{\lambda - \kappa + (1 - K_{ND})F_{ND}^{(\kappa, \lambda)}\} \quad (\text{B.13})$$

The ratio of (B.12a) to (B.13) approximates $E[\hat{f}]$ and is shown in Eqn. 2a.

Appendix C. Expected value of R_N

This method estimates the fraction, m_N , of Neanderthal gene flow into Eurasians. It uses genomes sampled from five populations: African, A , Eurasian, E , Neanderthal, N , Denisovan, D , and chimpanzee, C . As usual, we use the corresponding lower-case letters to represent genomes sampled from these populations. The method assumes that these populations are related as shown in Fig. 3. Although five populations are involved, only four are compared in the numerator, and a different four are compared in the denominator. In each panel of the figure, dashed lines indicate the sample that is ignored.

R_N is defined in Eqn. 3, which is equivalent to the definition of Patterson et al. (2010b, Eqn. S8.3). As discussed in section 3.2, we will consider a model in which the Eurasian population received gene flow from Neanderthals at time δ and from Denisovans at time α . A fraction m_N of the Eurasian gene pool derives from Neanderthal admixture, and a fraction m_D derives from Denisovan admixture. The remaining fraction, $(1 - m_N)(1 - m_D)$, is “native”—it descends from the ancestral population AE , of modern humans.

Table C.6: Contributions to each site pattern for the numerator of R_N . “Ref” refers to equations in Appendix C.1.

Coal.	$P_i B_i$	Ref
<i>Site Pattern ae only:</i>		
(ζ, λ)	$(1 - m_N)(1 - m_D)\{\lambda - \zeta + (1 - K_{AE})F_{AE}^{(\zeta, \lambda)}\}$	C.6
<i>Site Pattern de only:</i>		
(α, κ)	$m_D\{\kappa - \alpha + (\lambda - \kappa + 1 - K_D)F_D^{(\alpha, \kappa)}\}$	C.1
(κ, λ)	$m_D S_D^{(\alpha, \kappa)}\{\lambda - \kappa + (1 - K_{ND})F_{ND}^{(\kappa, \lambda)}\}$	C.2
(κ, λ)	$m_N(1 - m_D)\{\lambda - \kappa + (1 - K_{ND})F_{ND}^{(\kappa, \lambda)}\}$	C.4
<i>All Three Site Patterns:</i>		
$> \lambda$	$m_D S_D^{(\alpha, \kappa)} S_{ND}^{(\kappa, \lambda)} / 3$	C.3
$> \lambda$	$m_N(1 - m_D) S_{ND}^{(\kappa, \lambda)} / 3$	C.5
$> \lambda$	$(1 - m_N)(1 - m_D) S_{AE}^{(\zeta, \lambda)} / 3$	C.7

Appendix C.1. Numerator of R_N

The numerator of R_N does not involve an archaic genome. Nonetheless, we cannot ignore the Neanderthal and Denisovan populations, because a fraction of Eurasian ancestry flows through them. In the outline below, each item deals with one of the ways in which coalescent events can be distributed within the population tree shown in Fig. 3. Results are summarized in table C.6.

1 e arrived by gene flow from Denisovans.

1.1 e and d coalesce during (α, κ) , within D . Contributes to site pattern de only. The argument in Appendix A.3 gives $P = m_D F_D^{(\alpha, \kappa)}$; $B = \lambda - \kappa + 1 - K_D + (\kappa - \alpha)/F_D^{(\alpha, \kappa)}$.

$$PB = m_D\{\kappa - \alpha + (\lambda - \kappa + 1 - K_D)F_D^{(\alpha, \kappa)}\} \quad (C.1)$$

1.2 e and d coalesce during (κ, λ) , within ND . Contributes to site pattern de only. $P = m_D S_D^{(\alpha, \kappa)} F_{ND}^{(\kappa, \lambda)}$; $B = 1 - K_{ND} + (\lambda - \kappa)/F_{ND}^{(\kappa, \lambda)}$. Argument as in Appendix A.3.

$$PB = m_D S_D^{(\alpha, \kappa)}\{\lambda - \kappa + (1 - K_{ND})F_{ND}^{(\kappa, \lambda)}\} \quad (C.2)$$

1.3 First coalescent event is prior to time λ , in the ancestral human population. Contributes to all three site patterns. $P = m_D S_D^{(\alpha, \kappa)} S_{ND}^{(\kappa, \lambda)} / 3$; $B = 1$. Argument as in Appendix A.4.

$$PB = m_D S_D^{(\alpha, \kappa)} S_{ND}^{(\kappa, \lambda)} / 3 \quad (C.3)$$

2 e arrived by gene flow from Neanderthals.

2.1 e and d coalesce during (κ, λ) within ND . Contributes to site pattern de only. $P = m_N(1 - m_D)F_{ND}^{(\kappa, \lambda)}$; $B = 1 - K_{ND} + (\lambda - \kappa)/F_{ND}^{(\kappa, \lambda)}$.

$$PB = m_N(1 - m_D)\{\lambda - \kappa + (1 - K_{ND})F_{ND}^{(\kappa, \lambda)}\} \quad (C.4)$$

Argument as in Appendix A.3.

2.2 First coalescent event is prior to λ , in the ancestral population. Contributes to all three site patterns. $P = m_N(1 - m_D)S_{ND}^{(\kappa, \lambda)} / 3$; $B = 1$.

$$PB = m_N(1 - m_D)S_{ND}^{(\kappa, \lambda)} / 3 \quad (C.5)$$

Argument as in Appendix A.4.

3 e is native.

3.1 a and e coalesce during (ζ, λ) within AE . Contributes to site pattern ae only. $P = (1 - m_N)(1 - m_D)F_{AE}^{(\zeta, \lambda)}$; $B = 1 - K_{AE} + (\lambda - \zeta)/F_{AE}^{(\zeta, \lambda)}$.

$$PB = (1 - m_N)(1 - m_D)\{\lambda - \zeta + (1 - K_{AE})F_{AE}^{(\zeta, \lambda)}\} \quad (C.6)$$

Argument as in Appendix A.3.

3.2 First coalescent event is prior to λ , in the ancestral population. Contributes to all three site patterns. $P = (1 - m_N)(1 - m_D)S_{AE}^{(\zeta, \lambda)} / 3$; $B = 1$.

$$PB = (1 - m_N)(1 - m_D)S_{AE}^{(\zeta, \lambda)} / 3 \quad (C.7)$$

Argument as in Appendix A.4.

The last three rows of table C.6 refer to cases in which the first coalescent event occurs in the population ancestral to all humans, including archaics. These contribute equally to all three site patterns. Consequently, they disappear from the expected value of the numerator of R_N :

$$E[I_{de} - I_{ad}] \propto m_N(1 - m_D)\{\lambda - \kappa + (1 - K_{ND})F_{ND}^{(\kappa, \lambda)}\} + m_D\{\lambda - \alpha + (1 - K_D)F_D^{(\alpha, \kappa)} + (1 - K_{ND})S_D^{(\alpha, \kappa)}F_{ND}^{(\kappa, \lambda)}\} \quad (C.8)$$

This expression omits the constant multiplier, UL .

Appendix C.2. Denominator of R_N

The denominator of R_N includes a Neanderthal genome but does not include a Eurasian. For this reason, one-directional gene flow from archaics to Eurasians does not affect the calculation. The analysis in this case is very simple, so we will not record results in a table.

1 n and d coalesce during (κ, λ) within ND . Contributes to dn only. $P = F_{ND}$; $B = 1 - K_{ND} + (\lambda - \kappa)/F_{ND}^{(\kappa, \lambda)}$;

$$PB = \lambda - \kappa + (1 - K_{ND})F_{ND}^{(\kappa, \lambda)} \quad (C.9)$$

Argument as in Appendix A.3.

2 First coalescent event is prior to λ in the ancestral human population. Contributes to all three site patterns. $P = S_{ND}^{(\kappa, \lambda)} / 3$; $B = 1$;

$$PB = S_{ND}^{(\kappa, \lambda)} / 3 \quad (C.10)$$

Argument as in Appendix A.4.

These results imply that the denominator of R_N has expected value

$$E[J_{dn} - J_{ad}] \propto \lambda - \kappa + (1 - K_{ND})F_{ND}^{(\kappa, \lambda)} \quad (\text{C.11})$$

Using a ratio of expectations to approximate the expectation of a ratio, $E[R_N]$ is equal to the ratio of Eqns. C.8 and C.11.

Appendix D. Expected value of R_D

Patterson et al. (2010b, Eqn. S8.5) also define a second statistic, their R_{Denisova} , which we refer to as R_D . It assumes the setup shown in Fig. 5 and can be defined as in Eqn. 5. The numerator of R_D compares genomes sampled from populations S , E , V , and C . There are three site patterns— es , ev , and sv —that conform to the requirement that the chimpanzee carry the ancestral allele, and that the derived allele be present in two other populations. The numerator of R_D compares two of these. The denominator of R_D compares genomes from S , Y , D , and C , so the legal three site patterns are sy , ds , and dy . Of these, the denominator compares ds and sy .

This model assumes that archaic DNA entered modern populations via two episodes of gene flow. First, at time δ , there was gene flow from Neanderthals into the ancestor of all Eurasian populations. Just after this event, the fraction of Neanderthal DNA in modern human populations was m_N . Later, at time α , the Melanesian population experienced a second episode of gene flow, this time from Denisovans. A fraction m_D of Melanesian genes derive from Denisovans via this episode of gene flow. Of the remaining fraction, $1 - m_D$, a fraction m_N derives from Neanderthals, and another fraction, $1 - m_N$, is native. Thus, the DNA of modern Melanesians can be divided into three components: a fraction m_D is Denisovan, a fraction $m_N(1 - m_D)$ is Neanderthal, and a fraction $(1 - m_N)(1 - m_D)$ is native. In other Eurasian populations, there are only two components: a fraction m_N is Neanderthal, and the remaining fraction $1 - m_N$ is native.

Appendix D.1. Numerator of R_D

Each item below deals with one way in which coalescent events can be distributed in the population tree shown in the left panel of Fig. 5. Results are collected in table D.7.

1 v derives from Denisovan gene flow.

1.1 e derives from Neanderthal gene flow.

1.1.1 v and e coalesce during (κ, λ) , within ND . This case contributes to site pattern ev only. $P = m_N m_D F_{ND}^{(\kappa, \lambda)}$; $B = (\lambda - \kappa)/F_{ND}^{(\kappa, \lambda)} + 1 - K_{ND}$.

$$PB = m_N m_D \{\lambda - \kappa + (1 - K_{ND})F_{ND}^{(\kappa, \lambda)}\} \quad (\text{D.1})$$

Argument as in Appendix A.3.

1.1.2 *First coalescent event is prior to λ in the ancestral population.* Contributes to all three site patterns. $P = m_N m_D S_{ND}^{(\kappa, \lambda)}/3$; $B = 1$.

$$PB = m_N m_D S_{ND}^{(\kappa, \lambda)}/3 \quad (\text{D.2})$$

Argument as in Appendix A.4.

1.2 e is native.

1.2.1 e and s coalesce during (η, λ) , within $SYEV$. Contributes only to site pattern es . $P = m_D(1 - m_N)F_{SYEV}^{(\eta, \lambda)}$; $B = (\lambda - \eta)/F_{SYEV}^{(\eta, \lambda)} + 1 - K_{SYEV}$.

$$PB = m_D(1 - m_N) \{\lambda - \eta + (1 - K_{SYEV})F_{SYEV}^{(\eta, \lambda)}\} \quad (\text{D.3})$$

Argument as in Appendix A.3.

1.2.2 e and s coalesce prior to λ , within ancestral population. Contributes to all three site patterns. $P = m_D(1 - m_N)S_{SYEV}^{(\eta, \lambda)}/3$; $B = 1$.

$$PB = m_D(1 - m_N)S_{SYEV}^{(\eta, \lambda)}/3 \quad (\text{D.4})$$

Argument as in Appendix A.4.

2 v not from Denisova, and coalesces with e during (β, δ) within EV . Contributes to ev only. The frequency of such sites is $P = (1 - m_D)F_{EV}^{(\beta, \delta)}$. The branch length is

$$m_N(\lambda + v) + (1 - m_N)(\eta + x) - \beta - w$$

where v is the coalescence time in the ancestral human population and therefore has expectation 1. Variable x is the coalescence time in $SYEV$ and has expectation $T_{SYEV}^{(\eta)}$, as explained in Appendix A.2. Variable w is the conditional coalescence time, given that coalescence occurs within (β, δ) . Its expectation is

$$E[w|w < \delta - \beta] = K_{EV} - (\delta - \beta)S_{EV}^{(\beta, \delta)}/F_{EV}^{(\beta, \delta)}$$

as explained in Appendix A.1.

Assembling these pieces,

$$B = \eta - \delta + (\delta - \beta)/F_{SYEV}^{(\eta, \lambda)} + m_N \{\lambda - \eta + 1 - T_{SYEV}^{(\eta)}\} + T_{SYEV}^{(\eta)} - K_{EV}$$

and

$$PB = (1 - m_D) [\delta - \beta + F_{EV}^{(\beta, \delta)} \{\eta - \delta + m_N(\lambda - \eta) + m_N(1 - T_{SYEV}^{(\eta)}) + T_{SYEV}^{(\eta)} - K_{EV}\}] \quad (\text{D.5})$$

3 v derives from N .

3.1 e derives from N .

Table D.7: Contributions to each site pattern for the numerator of R_D . “Ref” refers to explanations in numbered paragraphs of Appendix D.1.

Coalescence	$P_i B_i$	Ref
<i>Site Pattern es only:</i>		
(η, λ)	$m_D(1 - m_N)\{\lambda - \eta + (1 - K_{SYEV})F_{SYEV}^{(\eta, \lambda)}\}$	D.3
(η, λ)	$m_N(1 - m_N)(1 - m_D)S_{EV}^{(\beta, \delta)}\{\lambda - \eta + (1 - K_{SYEV})F_{SYEV}^{(\eta, \lambda)}\}$	D.9
<i>Site Pattern ev only:</i>		
(κ, λ)	$m_N m_D\{\lambda - \kappa + (1 - K_{ND})F_{ND}^{(\kappa, \lambda)}\}$	D.1
(β, δ)	$(1 - m_D)[\delta - \beta + F_{EV}^{(\beta, \delta)}\{\eta - \delta + m_N(\lambda - \eta + 1 - T_{SYEV}^{(\eta)}) + T_{SYEV}^{(\eta)} - K_{EV}\}]$	D.5
(δ, κ)	$m_N^2(1 - m_D)S_{EV}^{(\beta, \delta)}\{\kappa - \delta + (\lambda - \kappa + 1 - K_N)F_N^{(\delta, \kappa)}\}$	D.6
(κ, λ)	$m_N^2(1 - m_D)S_{EV}^{(\beta, \delta)}S_N^{(\delta, \kappa)}\{\lambda - \kappa + (1 - K_{ND})F_{ND}^{(\kappa, \lambda)}\}$	D.7
(δ, η)	$(1 - m_N)^2(1 - m_D)S_{EV}^{(\beta, \delta)}\{\eta - \delta + (T_{SYEV}^{(\eta)} - K_{EV})F_{EV}^{(\delta, \eta)}\}$	D.13
<i>Site Pattern sv only:</i>		
(η, λ)	$m_N(1 - m_N)(1 - m_D)S_{EV}^{(\beta, \delta)}\{\lambda - \eta + (1 - K_{SYEV})F_{SYEV}^{(\eta, \lambda)}\}$	D.11
<i>All Three Site Patterns:</i>		
$> \lambda$	$m_N m_D S_{ND}^{(\kappa, \lambda)} / 3$	D.2
$> \lambda$	$m_D(1 - m_N)S_{SYEV}^{(\eta, \lambda)} / 3$	D.4
$> \lambda$	$m_N^2(1 - m_D)S_{EV}^{(\beta, \delta)}S_N^{(\delta, \kappa)}S_{ND}^{(\kappa, \lambda)} / 3$	D.8
$> \lambda$	$m_N(1 - m_N)(1 - m_D)S_{EV}^{(\beta, \delta)}S_{SYEV}^{(\eta, \lambda)} / 3$	D.10
$> \lambda$	$m_N(1 - m_N)(1 - m_D)S_{EV}^{(\beta, \delta)}S_{SYEV}^{(\eta, \lambda)} / 3$	D.12
$> \eta$	$\frac{1}{3}(1 - m_N)^2(1 - m_D)S_{EV}^{(\beta, \eta)}[K_{SYEV} + \frac{3}{2}(1 - K_{SYEV})S_{SYEV}^{(\eta, \lambda)} - \frac{1}{2}(1 - K_{SYEV})e^{-3(\lambda - \eta)/K_{SYEV}}]$	D.14

3.1.1 *e and v coalesce during (δ, κ) within N.* Contributes to *ev* only. $P = m_N^2(1 - m_D)S_{EV}^{(\beta, \delta)}F_N^{(\delta, \kappa)}$; $B = \lambda - \kappa + 1 - K_N + (\kappa - \delta)/F_N^{(\delta, \kappa)}$.

$$PB = m_N^2(1 - m_D)S_{EV}^{(\beta, \delta)}\{\kappa - \delta + (\lambda - \kappa + 1 - K_N)F_N^{(\delta, \kappa)}\} \quad (D.6)$$

Argument as in Appendix A.3.

3.1.2 *e and v coalesce during (κ, λ) within DN.* Contributes to *ev* only. $P = m_N^2(1 - m_D)S_{EV}^{(\beta, \delta)}S_N^{(\delta, \kappa)}F_{ND}^{(\kappa, \lambda)}$; $B = 1 - K_{ND} + (\lambda - \kappa)/F_{ND}^{(\kappa, \lambda)}$.

$$PB = m_N^2(1 - m_D)S_{EV}^{(\beta, \delta)}S_N^{(\delta, \kappa)}\{\lambda - \kappa + (1 - K_{ND})F_{ND}^{(\kappa, \lambda)}\} \quad (D.7)$$

Argument as in Appendix A.3.

3.1.3 *First coalescent event is prior to λ in the ancestral population.* Contributes to all three site patterns. $P = m_N^2(1 - m_D)S_{EV}^{(\beta, \delta)}S_N^{(\delta, \kappa)}S_{ND}^{(\kappa, \lambda)} / 3$; $B = 1$.

$$PB = m_N^2(1 - m_D)S_{EV}^{(\beta, \delta)}S_N^{(\delta, \kappa)}S_{ND}^{(\kappa, \lambda)} / 3 \quad (D.8)$$

Argument as in Appendix A.4.

3.2 *e is native.*

3.2.1 *e and s coalesce during (η, λ) within EVS.* Contributes to *es* only. $P = m_N(1 - m_N)(1 - m_D)S_{EV}^{(\beta, \delta)}F_{SYEV}^{(\eta, \lambda)}$; $B = 1 - K_{SYEV} + (\lambda - \eta)/F_{SYEV}^{(\eta, \lambda)}$.

$$PB = m_N(1 - m_N)(1 - m_D)S_{EV}^{(\beta, \delta)}\{\lambda - \eta + (1 - K_{SYEV})F_{SYEV}^{(\eta, \lambda)}\} \quad (D.9)$$

Argument as in Appendix A.3.

3.2.2 *First coalescent event is prior to λ within ancestral population.* Contributes to all three site patterns. $P = m_N(1 - m_N)(1 - m_D)S_{EV}^{(\beta, \delta)}S_{SYEV}^{(\eta, \lambda)} / 3$; $B = 1$.

$$PB = m_N(1 - m_N)(1 - m_D)S_{EV}^{(\beta, \delta)}S_{SYEV}^{(\eta, \lambda)} / 3 \quad (D.10)$$

Argument as in Appendix A.4.

4 *v is native.*

4.1 *e is from Neanderthal.*

4.1.1 *v and s coalesce during (η, λ) within EVS.* Contributes to *sv* only. $P = m_N(1 - m_N)(1 - m_D)S_{EV}^{(\beta, \delta)}F_{SYEV}^{(\eta, \lambda)}$; $B = 1 - K_{SYEV} + (\lambda - \eta)/F_{SYEV}^{(\eta, \lambda)}$.

$$PB = m_N(1 - m_N)(1 - m_D)S_{EV}^{(\beta, \delta)}\{\lambda - \eta + (1 - K_{SYEV})F_{SYEV}^{(\eta, \lambda)}\} \quad (D.11)$$

Argument as in Appendix A.3.

4.1.2 *First coalescent event is prior to λ within ancestral population.* Contributes to all three site patterns. $P = m_N(1 - m_N)(1 - m_D)S_{EV}^{(\beta, \delta)}S_{SYEV}^{(\eta, \lambda)} / 3$; $B = 1$.

$$PB = m_N(1 - m_N)(1 - m_D)S_{EV}^{(\beta, \delta)}S_{SYEV}^{(\eta, \lambda)} / 3 \quad (D.12)$$

Argument as in Appendix A.4.

4.2 *e is native.*

4.2.1 *e and v coalesce during (δ, η) within EV.* Contributes to *ev* only. $P = (1 - m_N)^2(1 - m_D)S_{EV}^{(\beta, \delta)}F_{EV}^{(\delta, \eta)}$; $B = (\eta - \delta)/F_{EV}^{(\delta, \eta)} + T_{SYEV}^{(\eta)} - K_{EV}$.

$$PB = (1 - m_N)^2(1 - m_D)S_{EV}^{(\beta, \delta)}\{\eta - \delta + (T_{SYEV}^{(\eta)} - K_{EV})F_{EV}^{(\delta, \eta)}\}. \quad (D.13)$$

Table D.8: Contributions to each site pattern for the denominator of R_D . “Ref” refers to explanations in numbered paragraphs of Appendix D.2.

Coalescence	$P_i B_i$	Ref
<i>Site Pattern sy only:</i>		
(η, λ)	$\lambda - \eta + (1 - K_{SYEV})F_{SYEV}^{(\eta, \lambda)}$	D.16
<i>All Three Site Patterns:</i>		
$> \lambda$	$S_{SYEV}^{(\eta, \lambda)}/3$	D.17

Argument as in Appendix A.3.

4.2.2 *First coalescent event is during (η, λ) within SYEV or during (λ, ∞) within the ancestral population.* Contributes to all three site patterns. $P = (1 - m_N)^2(1 - m_D)S_{EV}^{(\beta, \eta)}/3$. This case is unusual, in that, when we enter SYEV at time η , there are 3 lineages, and the hazard of a coalescent event is $3/K_{SYEV}$.

$$B = K_{SYEV} + \frac{3}{2}(1 - K_{SYEV})e^{-(\lambda - \eta)/K_{SYEV}} - \frac{1}{2}(1 - K_{SYEV})e^{-3(\lambda - \eta)/K_{SYEV}}$$

Under constant population size, this collapses to $B = 1$.

$$PB = \frac{1}{3}(1 - m_N)^2(1 - m_D)S_{EV}^{(\beta, \eta)}[K_{SYEV} + \frac{3}{2}(1 - K_{SYEV})S_{SYEV}^{(\eta, \lambda)} - \frac{1}{2}(1 - K_{SYEV})e^{-3(\lambda - \eta)/K_{SYEV}}] \quad (D.14)$$

The expected value of I_{es} is UL times the sum of terms in table D.7 that belong to site pattern es . A similar statement holds for I_{sv} . Terms that are common to both site patterns disappear from the expected difference, which therefore equals

$$E[I_{es} - I_{sv}] \propto m_D(1 - m_N)\{\lambda - \eta + (1 - K_{SYEV})F_{SYEV}^{(\eta, \lambda)}\} \quad (D.15)$$

ignoring the proportional multiplier, UL . This is the expected value of the numerator of R_D .

Appendix D.2. Denominator of R_D

The denominator of R_D is based on the right panel of Fig. 5.

- 1 *s and y coalesce during (η, λ) within SYEV.* Contributes to sy only. $P = F_{SYEV}^{(\eta, \lambda)}$; $B = 1 - K_{SYEV} + (\lambda - \eta)/F_{SYEV}^{(\eta, \lambda)}$.

$$PB = \lambda - \eta + (1 - K_{SYEV})F_{SYEV}^{(\eta, \lambda)} \quad (D.16)$$

Argument as in Appendix A.3.

- 2 *First coalescent event occurs prior to λ in the ancestral population, SYEVND.* Contributes to all three site patterns. $P = S_{SYEV}^{(\eta, \lambda)}/3$; $B = 1$.

$$PB = S_{SYEV}^{(\eta, \lambda)}/3 \quad (D.17)$$

Argument as in Appendix A.4.

These results are summarized in table D.8. The expected value of the denominator of R_D is

$$E[J_{sy} - J_{ds}] \propto \lambda - \eta + (1 - K_{SYEV})F_{SYEV}^{(\eta, \lambda)} \quad (D.18)$$

where we have ignored the proportional multiplier, UL . The expectation of R_D is approximately the ratio of (D.15) to (D.18), as shown in Eqn. 6 of section 3.3.

Appendix E. Expected value of p_D

In deriving the expected value of p_D , Reich et al. (2011) assume that changes in allele frequencies reflect genetic drift. They do not assume that drift has clock-like behavior. We will need clock-like behavior, however, in order to deal with admixture from Neanderthals and with non-simultaneous Denisovan admixture events. This section derives the expected value of p_D using a mutational clock.

Consider the population tree shown in figure 6. In that figure, W , X , and Y represent modern human populations, N and D represent archaic populations, and C is chimpanzee. Population W is an outgroup within modern humans, and X and Y represent two other modern human populations. The method assumes that Y received archaic gene flow, but W and X did not. At locus i , let w_i , x_i , y_i , and d_i represent the frequency of the derived allele in populations W , X , Y , and D .

Reich et al. (2011, Eqn. 1) define p_D as in our Eqn. 7. In the denominator of that expression, y'_i is the frequency within a fifth population, Y' . The method assumes that Y' occupies a position within the population tree that is similar to that of Y . In other words, the tree of W , X , Y' , and D has a topology identical to that shown in figure 6. To model ghost admixture, we allow for gene flow at time δ from the Neanderthal population into population Y and at time δ' into population Y' .

Dropping subscripts, each term in the numerator of p_D is $wx - wy - xd + yd$. Conditional on allele frequencies, wx is the probability that two random nucleotides, one drawn from W and the other from X , are both copies of the derived allele. The unconditional version of this probability, $E[wx]$, is the probability that a mutation occurred in a common ancestor of these two nucleotides. Because we exclude sites at which the chimpanzee carries the derived allele, this common ancestor must have lived after the separation with chimpanzees.

The probability of such a mutation depends on the length of the branch separating two coalescent events: one between the two hominin lineages and the other between

the hominin and chimpanzee lineages. If μ is the separation time of the hominin and chimpanzee populations, then the mean coalescence time of the hominin and chimpanzee gene lineages is $\mu + K_{CH}$, where the K_{CH} represents the coalescence time within the ancestral chimpanzee-hominin population.

The coalescence time of the two hominin lineages is $\zeta + z$, where $E[z] = T_{WXY}^{(\zeta)}$, as explained in Appendix A.2. In this notation,

$$\begin{aligned} E[wx] &\propto \mu + K_{CH} - \zeta - T_{WXY}^{(\zeta)} \\ E[wy] &\propto \mu + K_{CH} \\ &\quad - (m_D + m_N(1 - m_D))(\lambda + T_0^{(\lambda)}) \\ &\quad - (1 - m_N)(1 - m_D)(\zeta + T_{WXY}^{(\zeta)}) \\ E[xd] &\propto \mu + K_{CH} - \lambda - T_0^{(\lambda)} \\ E[yd] &\propto \mu + K_{CH} \\ &\quad - m_D(\alpha + T_D^{(\alpha)}) \\ &\quad - m_N(1 - m_D)(\kappa + T_{ND}^{(\kappa)}) \\ &\quad - (1 - m_N)(1 - m_D)(\lambda + T_0^{(\lambda)}) \end{aligned}$$

where $T_0^{(\lambda)}$ is the mean coalescence time for a pair of lineages that enters the ancestral human population at time λ , and we have omitted the constant multiplier UL . The numerator of p_D has expectation

$$\begin{aligned} E[wx - wy - xd + yd] &\propto \\ &\quad m_D(2\lambda - \zeta - \alpha) + m_N(1 - m_D)(2\lambda - \zeta - \kappa) \\ &\quad + m_D(2T_0^{(\lambda)} - T_{WXY}^{(\zeta)} - T_D^{(\alpha)}) \\ &\quad + m_N(1 - m_D)(2T_0^{(\lambda)} - T_{WXY}^{(\zeta)} - T_{ND}^{(\kappa)}) \quad (E.1) \end{aligned}$$

When population size is constant, all the T_i equal unity, and the last two lines of this expression disappear. That of the denominator is similar, except that we have α' , m'_N , and m'_D in place of α , m_N , and m_D . The ratio of these approximates $E[p_D]$ and is given in Eqn. 8.

Appendix F. Expected value of p_N

Dropping subscripts, each term in the numerator of Eqn. 9 is $ad - dx - an + nx$, and each term in the denominator is $ad - dm - an + mn$. The expected value of each product can be calculated as explained in Appendix E, using the assumptions in Fig. 7. Omitting the constant multiplier UL , the expectations of the various products

are

$$\begin{aligned} E[ad] &\propto \mu + K_{CH} - \lambda - T_0^{(\lambda)} \\ E[dx] &\propto \mu + K_{CH} - m_D(\alpha + T_D^{(\alpha)}) \\ &\quad - m_N(1 - m_D)(\kappa + T_{IMND}^{(\kappa)}) \\ &\quad - (1 - m_N)(1 - m_D)(\lambda + T_0^{(\lambda)}) \\ E[an] &\propto \mu + K_{CH} - \lambda - T_0^{(\lambda)} \\ E[nx] &\propto \mu + K_{CH} - m_D(\kappa + T_{IMND}^{(\kappa)}) \\ &\quad - m_N(1 - m_D)(\theta + T_{IMN}^{(\theta)}) \\ &\quad - (1 - m_N)(1 - m_D)(\lambda + T_0^{(\lambda)}) \\ E[dm] &\propto \mu + K_{CH} - \kappa - T_{IMND}^{(\kappa)} \\ E[mn] &\propto \mu + K_{CH} - \theta - T_{IMN}^{(\theta)} \end{aligned}$$

The expected numerator of p_N is

$$\begin{aligned} &m_N(1 - m_D)(\kappa - \theta + T_{IMND}^{(\kappa)} - T_{IMN}^{(\theta)}) \\ &\quad - m_D(\kappa - \alpha + T_{IMND}^{(\kappa)} - T_D^{(\alpha)}) \quad (F.1) \end{aligned}$$

The expected denominator is

$$\kappa - \theta + T_{IMND}^{(\kappa)} - T_{IMN}^{(\theta)}$$

The ratio of these, given in Eqn. 10, approximates the expectation of p_N .

Acknowledgements

We are grateful for comments from Elizabeth Cashdan, Henry Harpending, Flora Jay, and Montgomery Slatkin.

References

References

- Abi-Rached, L., Jobin, M. J., Kulkarni, S., McWhinnie, A., Dalva, K., Gragert, L., Babrzadeh, F., Gharizadeh, B., Luo, M., Plummer, F. A., et al., 2011. The shaping of modern human immune systems by multiregional admixture with archaic humans. *Science* 334 (6052), 89–94.
- Beerli, P., 2004. Effect of unsampled populations on the estimation of population sizes and migration rates between sampled populations. *Molecular Ecology* 13 (4), 827–836.
- Blum, M. G., Jakobsson, M., 2011. Deep divergences of human gene trees and models of human origins. *Molecular Biology and Evolution* 28 (2), 889–898.
- Bräuer, G., 1984. A craniological approach to the origin of anatomically modern *Homo sapiens* in Africa and implications for the appearance of modern Europeans. In: Smith, F., Spencer, F. (Eds.), *The Origins of Modern Humans: A World Survey of the Fossil Evidence*. Alan R. Liss, New York, pp. 327–410.
- Bräuer, G., 1989. The evolution of modern humans: A comparison of the African and non-African evidence. In: Mellars, P., Stringer, C. (Eds.), *The Human Revolution: Behavioural and Biological Perspectives on the Origins of Modern Humans*. Princeton University Press, Princeton, New Jersey, pp. 123–154.

- Cox, M. P., Mendez, F. L., Karafet, T. M., Pilkington, M. M., Kingan, S. B., Destro-Bisol, G., Strassmann, B. I., Hammer, M. F., 2008. Testing for archaic hominin admixture on the X chromosome: Model likelihoods for the modern human RRM2P4 region from summaries of genealogical topology under the structured coalescent. *Genetics* 178 (1), 427–437.
- Durand, E. Y., Johnson, P. L. F., Malaspinas, A.-S., Slatkin, M., 2010. Fraction of non-African genomes likely to be of Neandertal ancestry. Supplementary Note 19 of Green et al. (2010).
- Durand, E. Y., Patterson, N., Reich, D., Slatkin, M., 2011. Testing for ancient admixture between closely related populations. *Molecular Biology and Evolution* 28 (8), 2239–2252.
- Durand, E. Y., Slatkin, M., 2010. A population genetic model fit to the data. Supplementary Material 11 of Reich et al. (2010).
- Eriksson, A., Manica, A., 2012. Effect of ancient population structure on the degree of polymorphism shared between modern human populations and ancient hominins. *Proceedings of the National Academy of Sciences, USA* 109 (35), 13956–13960.
- Eriksson, A., Manica, A., 2014. The doubly-conditioned frequency spectrum does not distinguish between ancient population structure and hybridisation. *Molecular Biology and Evolution* 31 (6), 1618–1621.
- Eswaran, V., Harpending, H., Rogers, A. R., 2005. Genomics refutes an exclusively African origin of humans. *Journal of Human Evolution* 49, 1–18.
- Evans, P. D., Gilbert, S. L., Mekel-Bobrov, N., Vallender, E. J., Anderson, J. R., Vaez-Azizi, L. M., Tishkoff, S. A., Hudson, R. R., Lahn, B. T., 2005. Microcephalin, a gene regulating brain size, continues to evolve adaptively in humans. *Science* 309, 1717–1720.
- Gravel, S., Henn, B. M., Gutenkunst, R. N., Indap, A. R., Marth, G. T., Clark, A. G., Yu, F., Gibbs, R. A., Project, T. G., Bustamante, C. D., 2011. Demographic history and rare allele sharing among human populations. *Proceedings of the National Academy of Sciences* 108 (29), 11983–11988.
- Green, R. E., Krause, J., Briggs, A. W., Maricic, T., Stenzel, U., Kircher, M., Patterson, N., Li, H., Zhai, W., Fritz, M. H.-Y., Hansen, N. F., Durand, E. Y., Malaspinas, A.-S., Jensen, J. D., Marques-Bonet, T., Alkan, C., Prüfer, K., Meyer, M., Burbano, H. A., Good, J. M., Schultz, R., Aximu-Petri, A., Butthof, A., Höber, B., Höffner, B., Siegemund, M., Weihmann, A., Nusbaum, C., Lander, E. S., Russ, C., Novod, N., Affourtit, J., Egholm, M., Verna, C., Rudan, P., Brajkovic, D., Kucan, v., Gušić, I., Doronichev, V. B., Golovanova, L. V., Lalueza-Fox, C., de la Rasilla, M., Fortea, J., Rosas, A., Schmitz, R. W., Johnson, P. L. F., Eichler, E. E., Falush, D., Birney, E., Mullikin, J. C., Slatkin, M., Nielsen, R., Kelso, J., Lachmann, M., Reich, D., Pääbo, S., 2010. A draft sequence of the Neandertal genome. *Science* 328 (5979), 710–722.
- Hammer, M. F., Woerner, A. E., Mendez, F. L., Watkins, J. C., Wall, J. D., 2011. Genetic evidence for archaic admixture in Africa. *Proceedings of the National Academy of Sciences, USA* 108 (37), 15123–15128.
- Harris, K., Nielsen, R., 2013. Inferring demographic history from a spectrum of shared haplotype lengths. *PLoS Genetics* 9 (6), e1003521.
- Howells, W. W., 1976. Explaining modern man: Evolutionists versus migrationists. *Journal of Human Evolution* 5, 477–495.
- Hudson, R. R., 1990. Gene genealogies and the coalescent process. In: Futuyma, D., Antonovics, J. (Eds.), *Oxford Surveys in Evolutionary Biology*. Vol. 7. Oxford University Press, Oxford, pp. 1–44.
- Hudson, R. R., 1992. Gene trees, species trees, and the segregation of ancestral alleles. *Genetics* 131, 509–512.
- Mendez, F. L., Watkins, J. C., Hammer, M. F., 2012. Global genetic variation at OAS1 provides evidence of archaic admixture in Melanesian populations. *Molecular Biology and Evolution* 29 (6), 1513–1520.
- Meyer, M., Kircher, M., Gansauge, M.-T., Li, H., Racimo, F., Mallick, S., Schraiber, J. G., Jay, F., Prüfer, K., de Filippo, C., Sudmant, P. H., Alkan, C., Fu, Q., Do, R., Rohland, N., Tandon, A., Siebauer, M., Green, R. E., Bryc, K., Briggs, A. W., Stenzel, U., Dabney, J., Shendure, J., Kitzman, J., Hammer, M. F., Shunkov, M. V., Derevianko, A. P., Patterson, N., Andrs, A. M., Eichler, E. E., Slatkin, M., Reich, D., Kelso, J., Pääbo, S., 2012. A high-coverage genome sequence from an archaic Denisovan individual. *Science* 338 (6104), 222–226.
- Moorjani, P., Patterson, N., Hirschhorn, J. N., Keinan, A., Hao, L., Atzmon, G., Burns, E., Ostrer, H., Price, A. L., Reich, D., 2011. The history of African gene flow into Southern Europeans, Levantines, and Jews. *PLoS Genetics* 7 (4), e1001373.
- Nordborg, M., 1998. On the probability of Neanderthal ancestry. *American Journal of Human Genetics* 63 (4), 1237–1240.
- Pamilo, P., Nei, M., 1988. Relationships between gene trees and species trees. *Molecular Biology and Evolution* 5 (5), 568–583.
- Patterson, N., Hansen, N., Mullikin, J., Reich, D., 2010a. Neandertals are more closely related to non-Africans than to Africans. Supplementary Note 15 of Green et al. (2010).
- Patterson, N., Li, H., Mallick, S., Reich, D., 2010b. Denisovans share more derived alleles with Melanasi-ans than with other groups. Supplementary Note 8 of Reich et al. (2010).
- Patterson, N., Mallick, S., Reich, D., 2012a. D-statistics and interbreeding between archaic and modern humans. Supplementary Material 11 of Meyer et al. (2012).
- Patterson, N., Mallick, S., Reich, D., 2014. Neandertal population relationships and mixture proportions. Supplementary Information 14 of Prüfer et al. (2014).
- Patterson, N., Moorjani, P., Luo, Y., Mallick, S., Rohland, N., Zhan, Y., Genschoreck, T., Webster, T., Reich, D., 2012b. Ancient admixture in human history. *Genetics* 192 (3), 1065–1093.
- Patterson, N., Reich, D., 2010. Model-free estimate of the proportion of Neandertal ancestry in present-day non-Africans. Supplementary Note 18 of Green et al. (2010).
- Pinhasi, R., Higham, T. F., Golovanova, L. V., Doronichev, V. B., 2011. Revised age of late Neandertal occupation and the end of the Middle Paleolithic in the northern Caucasus. *Proceedings of the National Academy of Sciences, USA* 108 (21), 8611–8616.
- Plagnol, V., Wall, J. D., 2006. Possible ancestral structure in human populations. *PLoS Genetics* 2 (7), e105.
- Prüfer, K., Racimo, F., Patterson, N., Jay, F., Sankararaman, S., Sawyer, S., Heinze, A., Renaud, G., Sudmant, P. H., de Filippo, C., Li, H., Mallick, S., Dannemann, M., Fu, Q., Kircher, M., Kuhlwilm, M., Lachmann, M., Meyer, M., Ongyerth, M., Siebauer, M., Theunert, C., Tandon, A., Moorjani, P., Pickrell, J., Mullikin, J. C., Vohr, S. H., Green, R. E., Hellmann, I., Johnson, P. L. F., Blanche, H., Cann, H., Kitzman, J. O., Shendure, J., Eichler, E. E., Lein, E. S., Bakken, T. E., Golovanova, L. V., Doronichev, V. B., Shunkov, M. V., Derevianko, A. P., Viola, B., Slatkin, M., Reich, D., Kelso, J., Pääbo, S., 2014. The complete genome sequence of a Neandertal from the Altai Mountains. *Nature* 505 (7481), 43–49.
- Reich, D., Green, R., Kircher, M., Krause, J., Patterson, N., Durand, E., Viola, B., Briggs, A., Stenzel, U., Johnson, P., et al., 2010. Genetic history of an archaic hominin group from Denisova Cave in Siberia. *Nature* 468 (7327), 1053–1060.
- Reich, D., Patterson, N., Kircher, M., Delfin, F., Nandineni, M. R., Pugach, I., Ko, A. M.-S., Ko, Y.-C., Jinam, T. A., Phipps, M. E., Saitou, N., Wollstein, A., Kayser, M., Pääbo, S., Stoneking, M., 2011. Denisova admixture and the first modern human dispersals into Southeast Asia and Oceania. *American Journal of Human Genetics* 89 (4), 516–528.
- Sankararaman, S., Patterson, N., Li, H., Pääbo, S., Reich, D., 2012. The date of interbreeding between Neandertals and modern humans. *PLoS Genetics* 8 (10), e1002947.
- Slatkin, M., 2005. Seeing ghosts: The effect of unsampled populations on migration rates estimated for sampled populations. *Molecular Ecology* 14 (1), 67–73.
- Slatkin, M., Pollack, J. L., 2008. Subdivision in an ancestral species creates asymmetry in gene trees. *Molecular Biology and Evolution* 25 (10), 2241–2246.
- Smith, F. H., Falsetti, A. B., Donnelly, S. M., 1989. Modern human origins. *Yearbook of Physical Anthropology* 32, 35–68.
- Stoneking, M., 1993. DNA and recent human evolution. *Evolutionary*

- Anthropology 2 (2), 60–73.
- Stringer, C. B., Andrews, P., March 1988. Genetic and fossil evidence for the origin of modern humans. *Science* 239, 1263–1268.
- Trinkaus, E., 2005. Early modern humans. *Annual Review of Anthropology* 34, 207–230.
- Veeramah, K. R., Hammer, M. F., 2014. The impact of whole-genome sequencing on the reconstruction of human population history. *Nature Reviews Genetics* 15 (3), 149–162.
- Wall, J., Hammer, M., 2006. Archaic admixture in the human genome. *Current Opinion in Genetics & Development* 16 (6), 606–610.
- Wall, J. D., 2000. Detecting ancient admixture in humans using sequence polymorphism data. *Genetics* 154, 1271–1279.
- Wall, J. D., 2003. Estimating ancestral population sizes and divergence times. *Genetics* 163, 395–404.
- Wall, J. D., Lohmueller, K. E., Plagnol, V., 2009. Detecting ancient admixture and estimating demographic parameters in multiple human populations. *Molecular Biology and Evolution* 26 (8), 1823–1827.
- Wall, J. D., Yang, M. A., Jay, F., Kim, S. K., Durand, E. Y., Stevison, L. S., Gignoux, C., Woerner, A., Hammer, M. F., Slatkin, M., 2013. Higher levels of Neanderthal ancestry in East Asians than in Europeans. *Genetics* 194 (1), 199–209.
- Wolpoff, M. H., 1989. Multiregional evolution: The fossil alternative to Eden. In: Mellars, P., Stringer, C. (Eds.), *The Human Revolution: Behavioural and Biological Perspectives on the Origins of Modern Humans*. Princeton University Press, Princeton, New Jersey, pp. 62–108.
- Yang, M. A., Malaspina, A.-S., Durand, E. Y., Slatkin, M., 2012. Ancient structure in Africa unlikely to explain Neanderthal and non-African genetic similarity. *Molecular Biology and Evolution* 29 (10), 2987–2995.

Bias in Estimators of Archaic Admixture Supplementary Materials

Alan R. Rogers*

Ryan J. Bohlender

December 23, 2014

S1 Validating theoretical formulas

To check for errors in algebraic formulas, we developed software to simulate the components of each estimator. These simulations generate gene genealogies by running a coalescent process constrained by assumptions involving the population tree (branch lengths as well as topology), admixture events (timing as well as level of gene flow), and the size of each population.

Our goal was to estimate the expected values of the numerator and denominator of each estimator—not the full sampling distributions. Accordingly, we treated loci as independent and simulated the genealogical process but not the mutational process. This approach provides accurate estimates of expected values but underestimates sampling variances.

For statistics, \hat{f} , R_N , R_D , p_N , and Q , we set the fraction of primary admixture at 0.03. For p_D , we assumed that m_D equals 0.06 in the numerator but 0.03 in the denominator. All other parameters were chosen at random. These randomized parameters included population sizes,

branch lengths in the population tree, the timing of admixture events, and the level of ghost admixture.

For each statistic, we considered 50 random sets of parameter values. For each set, we estimated the statistic and its component parts both by simulation and from the theoretical formulas given in the main text. Simulated values are plotted against theoretical ones in Figs. S1–S6. In each case, the points fall close to a 45-degree line through the origin, indicating good agreement between theory and simulation.

If these statistics were unbiased estimators of the level of primary admixture, we would expect \hat{f} , R_N , R_D , p_N , and Q to cluster near the level, 0.03, of primary admixture. We would expect p_D to cluster near 2, the ratio of primary admixture in the numerator to that in the denominator. (These targets are shown as dotted vertical lines in the first panel of each figure below.)

This clustering is present, however, only in R_D and p_N (Figs. S3 and S5). The values of the other statistics are distributed along the 45-degree line, showing that they are sensitive to variation in parameter values. There are several outlying points in the graphs of the two F_4 -ratio statistics, p_D and p_N (Figs. S4 and S5). These outliers are remarkable, because each point on

*Dept. of Anthropology, 270 S 1400 E, University of Utah, Salt Lake City, Utah 84112. rogers@anthro.utah.edu

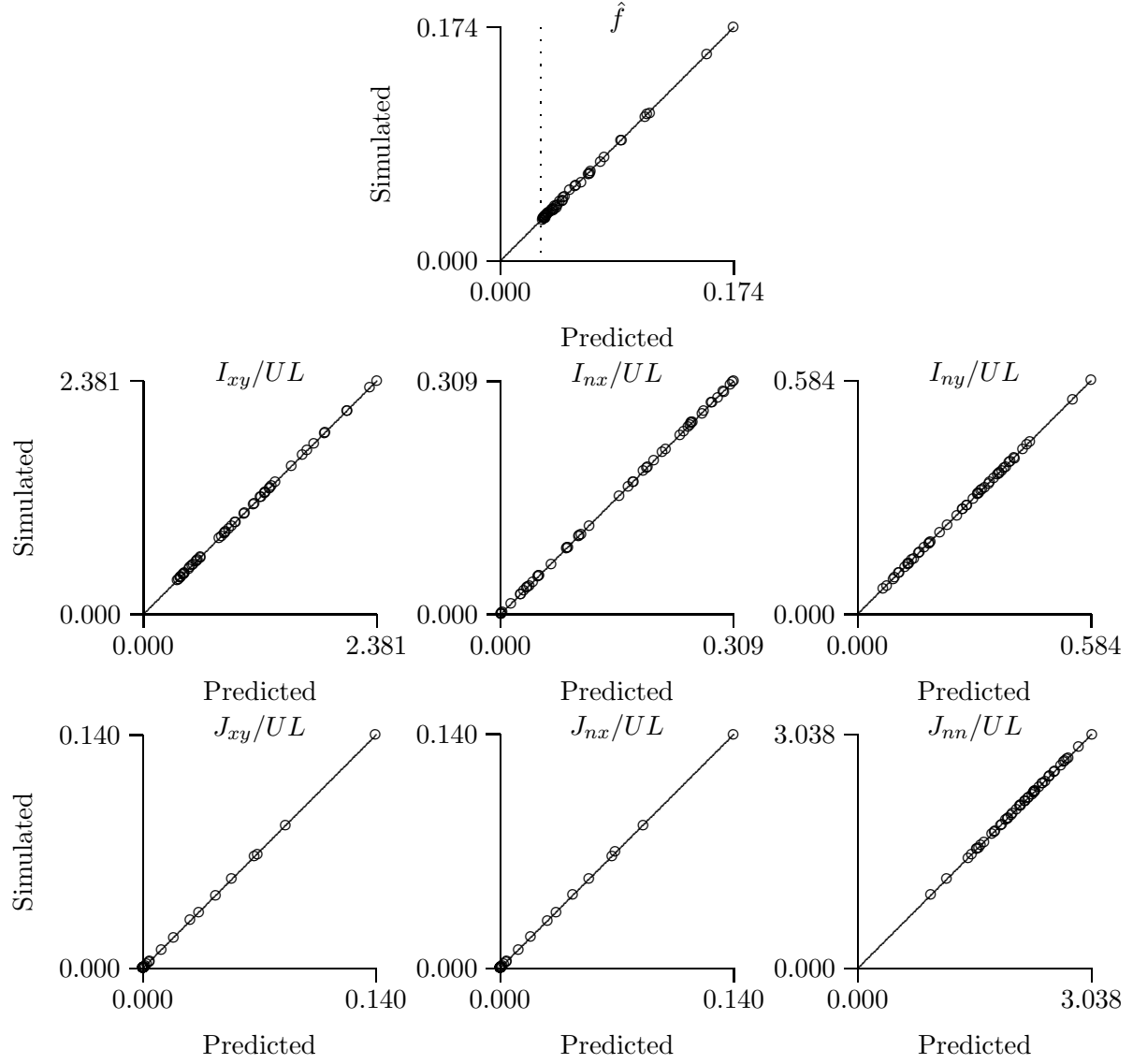


Figure S1: Simulated versus predicted values of \hat{f} and its components. Simulations used 10^6 iterations and assume $m_N = 0.03$. All other parameters were chosen at random for each of 50 simulations. Simulated and predicted values are equal along the solid 45-degree lines.

these graphs is an average across 10^8 iterations. The sampling distributions of these statistics must have very broad tails, at least for some sets of parameter values.

The software used in these calculations is included in the Supplementary Materials.

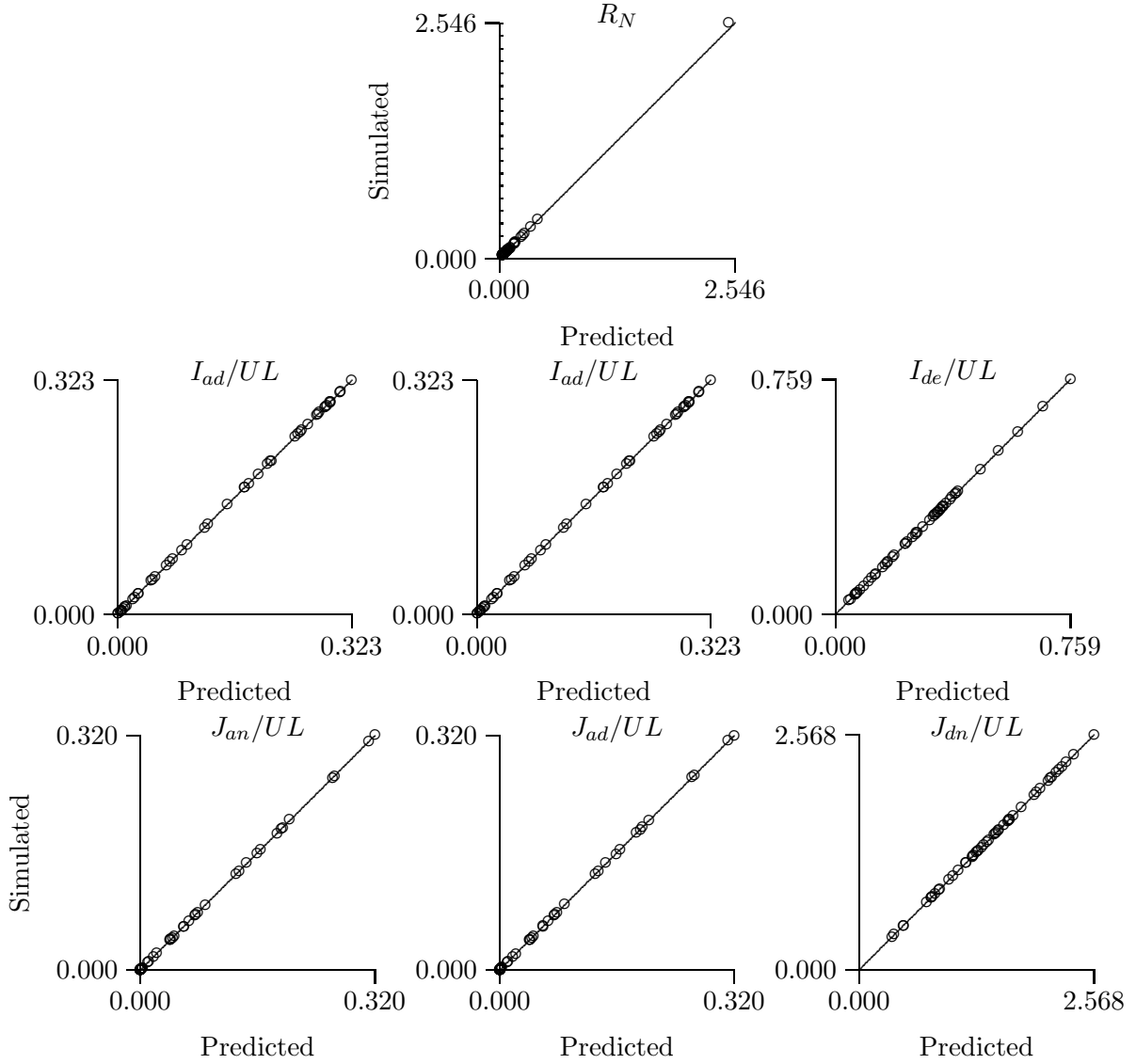


Figure S2: Simulated versus predicted values of R_N and its components. Simulations used 10^6 iterations and assume $m_N = 0.03$. All other parameters were chosen at random for each of 50 simulations. Simulated and predicted values are equal along the solid 45-degree lines.

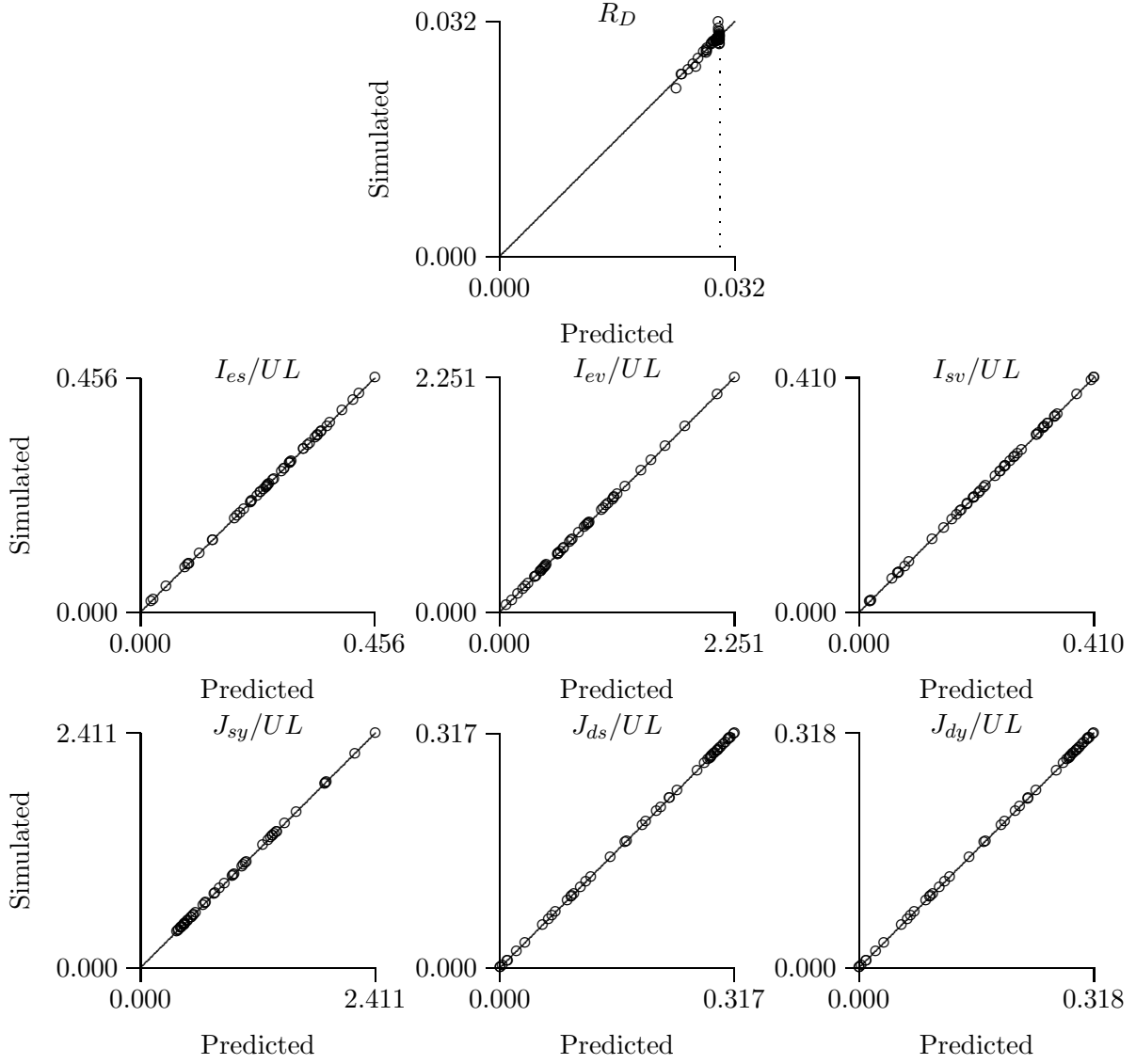


Figure S3: Simulated versus predicted values of R_D and its components. Simulations used 10^8 iterations and assume $m_D = 0.03$. All other parameters were chosen at random for each of 50 simulations. Simulated and predicted values are equal along the solid 45-degree lines.

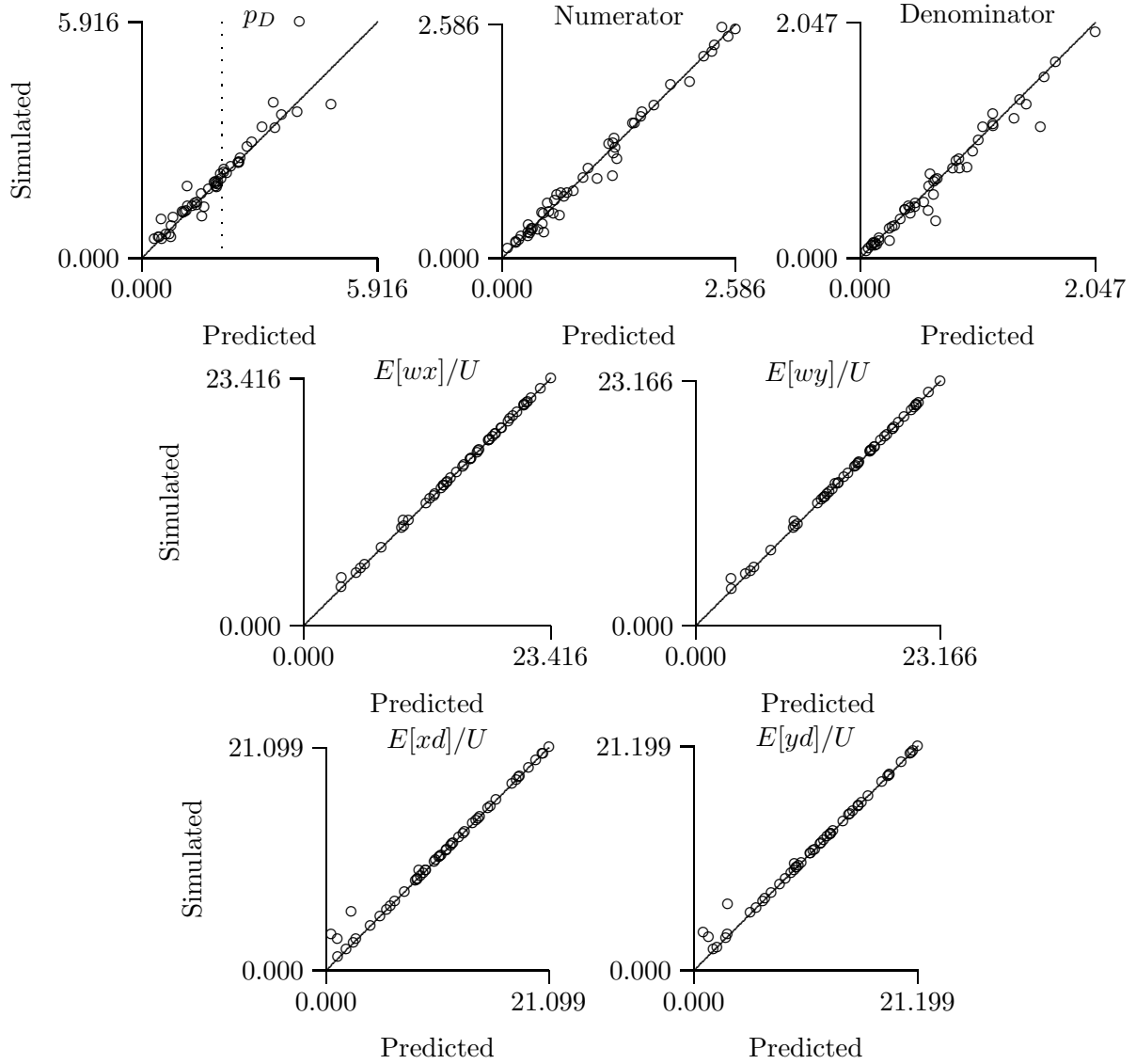


Figure S4: Simulated versus predicted values of p_D and its components. Simulations used 10^8 iterations and assume $m_D = 0.06$ and $m'_D = 0.03$. All other parameters were chosen at random for each of 50 simulations. Simulated and predicted values are equal along the solid 45-degree lines.

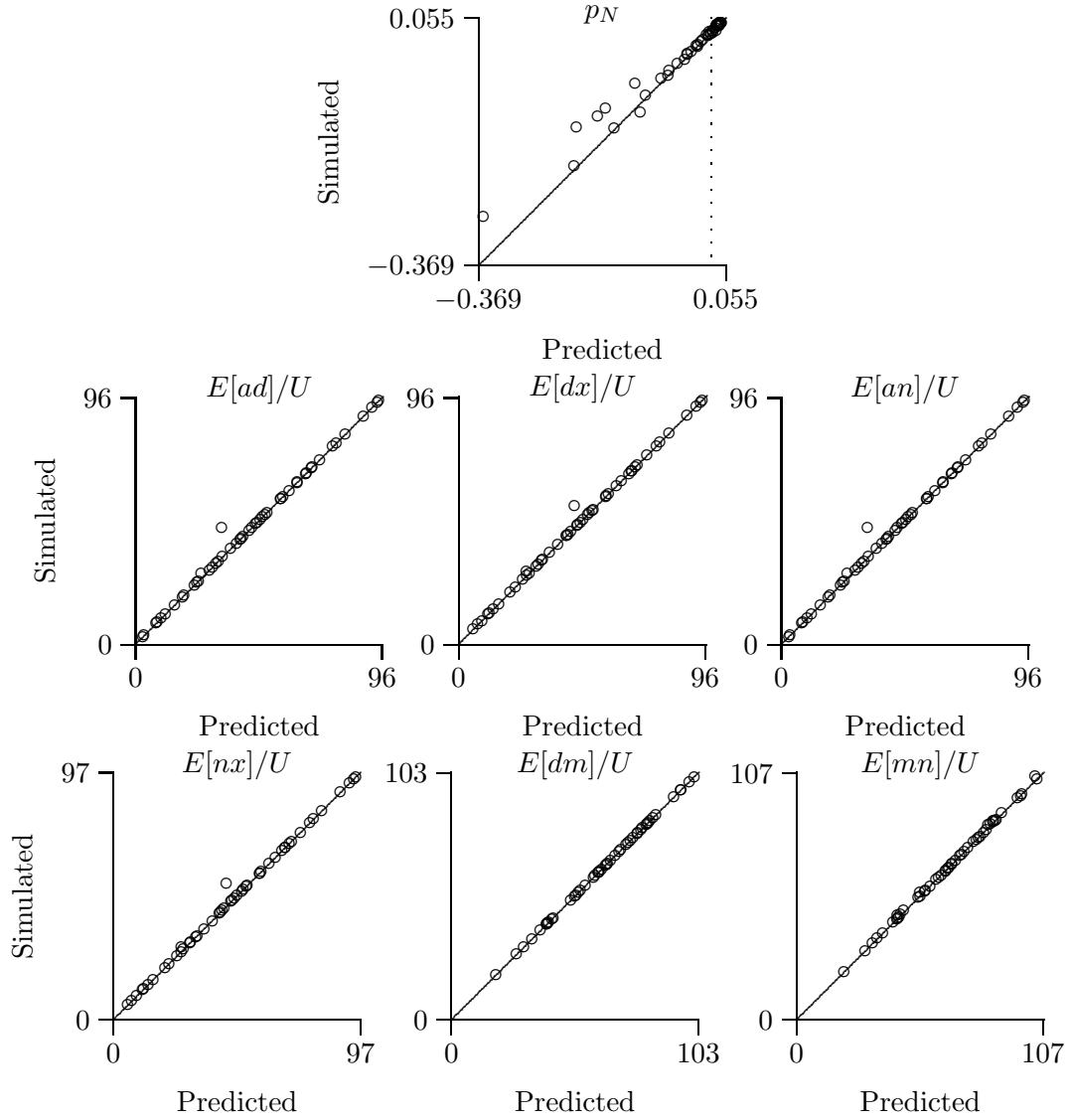


Figure S5: Simulated versus predicted values of p_N and its components. Simulations used 10^8 iterations and assume $m_N = 0.03$. All other parameters were chosen at random for each of 50 simulations. Simulated and predicted values are equal along the solid 45-degree lines.

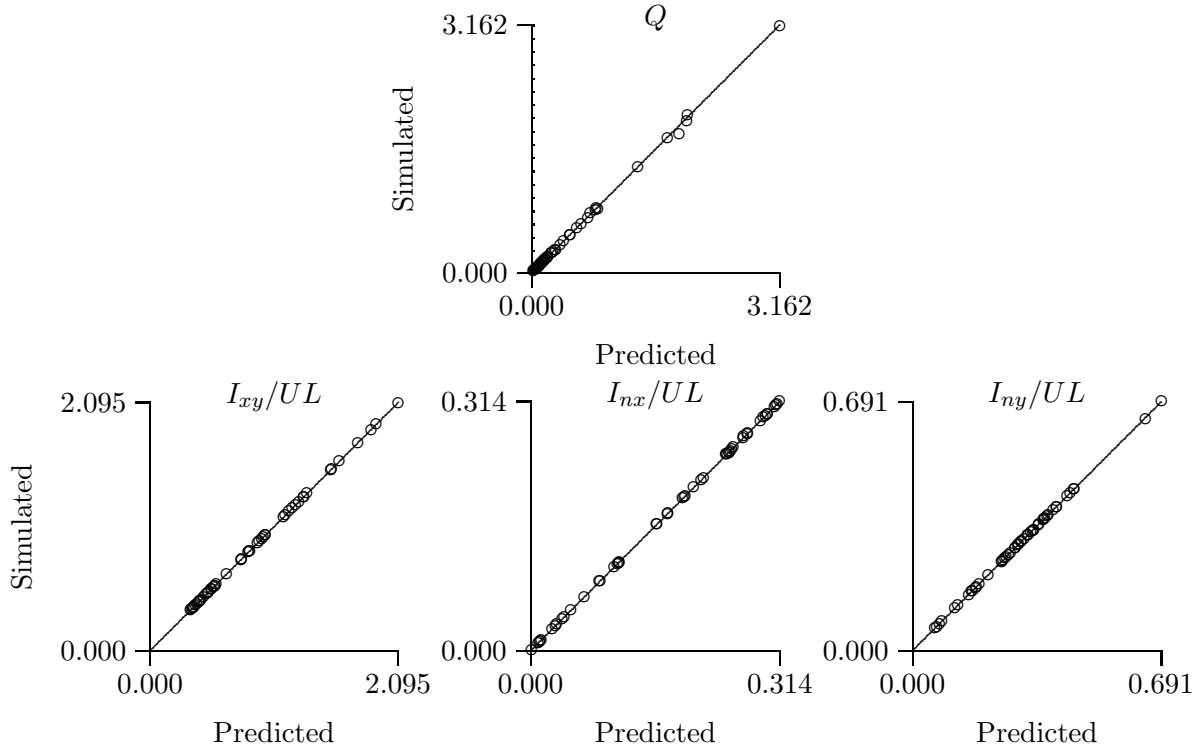


Figure S6: Simulated versus predicted values of Q and its components. Simulations used 10^6 iterations and assume $m_N = 0.03$. All other parameters were chosen at random for each of 50 simulations. Simulated and predicted values are equal along the solid 45-degree lines.